STUDY OF PHOTOPRODUCTION ON THE REACTION $\gamma p \rightarrow \eta p$

USING MONTE CARLO SIMULATION

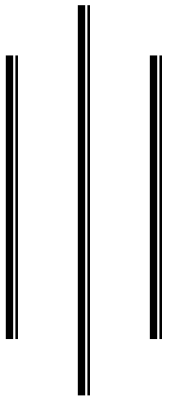

A Dissertation Submitted to the

Patan Multiple Campus, Department of Physics, T. U.

Patandhoka, Lalitpur, Nepal

In the partial fulfillment of the requirement for the

DEGREE OF MASTER OF SCIENCE IN PHYSICS

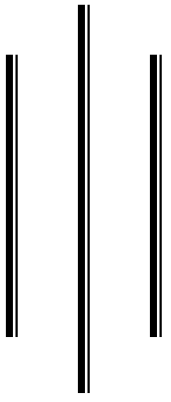

By: **Krishna Prasad Aryal**

Symbol No.:- 5229/2066

T.U. Regd. No.:- 5-1-49-61-99

Email: - krishnaaryal_s@yahoo.com

2012

Recommendation

It is certified that Mr. **Krishna Prasad Aryal** has carried out the dissertation work entitled **"STUDY OF PHOTOPRODUCTION ON THE REACTION $\gamma p \rightarrow \eta p$ USING MONTE CARLO SIMULATION"** under my supervision.

I recommend the dissertation for the partial fulfillment of the requirement for the degree of **Master of Science in Physics** at Tribhuvan University**.**

Dr. Kabiraj Bantawa

Lecturer

Trichandra Multiple Campus

Kathmandu, Nepal

Date: _____

Evaluation

We certify that we have read this dissertation entitled "**STUDY OF PHOTOPRODUCTION ON THE REACTION $\gamma p \rightarrow \eta p$ USING MONTE CARLO SIMULATION"** and in our opinion, it fulfills all the specified criteria, in the scope and quality, as a dissertation for the partial fulfillment of the requirement for the degree of Master of Science in physics at Tribhuvan University.

Evaluation committee

_____ _____

Dr. Kabiraj Bantawa
Supervisor

Mr. G.B. Shrestha
Co-ordinator : Department of Physics
Patan Multiple Campus
Lalitpur,Nepal

_____ _____

External Examiner

Internal Examiner

Date:

Acknowledgement

Various people who assisted me directly or indirectly trigger successful completion of this thesis work. First and the foremost I would like to pay gratitude to my inspiring and very cooperative supervisor Dr.Kabiraj Bantawa .He always encouraged me to choose such an interesting topic of Nuclear Physics focused on "study of photoproduction on the reaction $\gamma p \rightarrow \eta p \rightarrow \gamma\gamma p$" and supported me to complete this thesis work. Discussion with him had always generated a new site into the subject matter. Without his scientific vision, continuous encouragement and correct approach to understand the subject matter of present research the dissertation would never have taken this present shape. During the period of my work, I got an opportunity to get familiar with several software.

I extend my heartfelt thank to Head of department of physics Mr. G.B. Shrestha, Mr. Prakashman Shrestha, Mr.Homanath Poudyal, Prof. Dr. Jiwanjyoti Nakarmi, and all professors and lecturers of department of Physics who regularly encouraged me to work on the subject matter and inculcated an inner strengths.

My special thanks go to Dr. Bantawa for his suggestions and precious assistances in finding out the journals and article on Nuclear Physics. Furthermore, I must thank my senior Vikash Kaphle and my brother Shreedhar who always helped me to solve the problems arose during the use of software. I wish to express my sincere thanks to my collegues Gopal Gnawali, Ramchandra Adhikari, Suman Gahire, Pusparaj Sharma, Shreekumar B.C. my brothers Nabin, Tirtha, Pradeep and all the friends for their constant encouragements, supports and immense assistances.

Finally, this work would not have been possible without the support of my family. They have been a constant source of encouragement over the past few years and I dedicate this thesis to them. This entire works reflects their love, care and blessings.

Krishna Pd. Aryal

Abstract

This dissertation presents a study of photoproduction of *eta* meson from **Monte Carlo Simulation method**. It provides virtual experimental set up for the study of photoproduction reaction $\gamma p \rightarrow \eta p \rightarrow \gamma\gamma p$. This simulation includes event generation, particle identification and reconstruction of events. Depending upon the threshold energy for η photoproduction, this dissertation presents study of $\gamma p \rightarrow \eta p \rightarrow \gamma\gamma p$ in the energy range **735-≤Eγ≤1400 MeV**.

At first step, events for $\gamma p \rightarrow \eta p$ were generated by using *mkin* software. The generated events in the form of ROOT tree software include generation of eta meson, proton and two photons. Moreover, it contains generation of photon beam and generation of target vertex.

In second step, generated events were detected by using *cbsim* software. The detected events include identification of *eta meson*, outgoing *photons* and *proton*, vertex identification, detection of position of elements of NaI and BaF_2 crystal, detection of energy and momentum.

In third step, detected events were reconstructed by using *AcquRoot* software. These reconstructed events include invariant mass of *eta meson*, missing mass of *proton*, position of elements in *NaI crystal* and BaF_2 *crystal*. Invariant mass of *eta meson* was found approximately 550 MeV/c^2 and missing mass of *eta meson* or *proton mass* was found approximately 938 MeV/c^2, which is in close agreement with the previous simulation works.

The comparisons of our results with the previous simulation as well as experimental works show that our results found to be in close agreement with the previous simulation works.

Table of Contents

CHAPTER ONE

Introduction

1.1 Elementary particles

The problems concerning the *elementary particles* are today the focus of interest and of research for the experimental as well as the theoretical physicists. Experimental investigations of elementary particles involve some source of particles to study and some way of detecting those particles and measuring their behaviour. Many of the practical problems of such investigations are caused by the fact that many elementary particles are unstable. The classical *elementary particle*, the individual atom was nothing but the mass point of classical mechanics. The investigation of electromagnetic phenomena suggested that *the atom* had an internal structure. At that time, the typical photo-type of elementary particle was the *electron*. The problem of the dualistic nature of matter was resolved by the quantum theory of fields: the elementary particles are nothing but the quanta of a corresponding field. The study of elementary particles is basis to the understanding of radiation phenomena, or one may regard any kind of radiation as a flux of elementary particles.

In 1932, when **Chadwick** identified the neutron [1] and **Heisenberg** suggested that atomic nuclei consisted of *neutrons* and *protons* [2], it seemed as if **p, n** and $\mathbf{e^-}$ were sufficient to account for the structure of matter. Besides these there was the *photon*, the intermediary or field particle for electromagnetic forces, such as exist between *the nucleus and electrons* in the atom. If anti-matter exists, it would then be made of anti electrons, i.e. *protons*, *antiprotons* and *antineutrons* .Thus we see that seven particles could explain both matter and antimatter. In 1935, **Yukawa** postulated the existence of another particle, with a mass $\mathbf{m \simeq 200 m_e}$ as the field particle for the strong nuclear forces [3]. Recently the extensive studies made partly on high-energy cosmic ray particles and even more, with the help of high-energy accelerators have revealed the existence of numerous new nuclear particles. Apart from a dozen or so, the particles have very short lifetimes, very much less than $\mathbf{10^{-8}}$ **sec.** Therefore, they

cannot be considered as normal constituents of matter. They are characterized by the parameters: mass, spin, electric charge and magnetic moment. They have been described by such adjectives, as fundamental, strange and elementary, but none of these is quiet appropriate. The word fundamental implies that the particles are the basic building blocks of matter, but unstability of most of the particles indicates that the great majority are certainly not. It is true that their behaviour was strange in the early 1950, but it is much less now. For the want of better one the term elementary particles is now commonly used. These particles are elementary in much the same sense, as are the chemical elements [4].

1.2 Classification of elementary particles

Elementary particles are the fundamental constituents of all the matter in the universe. Fundamental particles are smallest things in the universe. The particles, which are structureless, indivisible and not regarded as made up of some other particles, are called *elementary particles* [4]. The elementary particles are separated into two general groups, called *bosons* and *fermions*. These two groups have different types of spin and their behaviour is controlled respectively by a different kind of statistics **(i.e. the Bose-statistic or the Fermi statistic)**. *Bosons* are particles with intrinsic angular momentum equal to an integral multiple of ħ. *Fermions* are all those particles in which the spin is half-integral. The most important difference between the two classes of particles is that there is no conservation law controlling the total number of bosons in the Universe, whereas the total number of *fermions* is strictly conserved [4, 5].

Boson is a term, which not only includes material particles but also includes those *quanta* and *photons*, which arise from interactions. Thus in the case of simple electromagnetic field the *bosons* are merely the light photons or X-ray photons. The *photon* has a mass of zero and spin of unity and is consequently described as a massless *boson*. A massless *boson*, called a *graviton* with a probable spin of two units has been postulated as a field particle for gravity. These *bosons*, created by the electromagnetic field, are essentially of one kind, while the *bosons* formed in the strong interaction are of three distinct kinds. First, there are those, which are known as *pions* or *π-meson* ($\boldsymbol{\pi^+, \pi^-, \pi^0}$). The second groups of *bosons* are much heavier than that

of pions, are known as *kaons or K-mesons* ($\mathbf{K^+}$, $\bar{K}$, $\mathbf{K^0}$, $\bar{K}^0$) and the third *eta meson* (η).

The *fermions* fall in two main classes, according to whether they are lighter than *mesons*, or heavier. Those in the lighter group are often called *leptons* (after the Greek word meaning light in weight), while those in the heavier group are called *baryons* (after the Greek word for heavy). The leptons are the *electrons, muons and neutrinos and their antiparticles*. These are all with masses less than the pions and their antiparticles and with spin half. *Leptons* interact weakly with other particles. The total number of *leptons* minus the total number of *anti-leptons* remains unchanged in all reactions and decay processes involving *leptons and anti-leptons*. The *baryons* consists of two nucleons with their *anti-particles* ($\mathbf{n^0}$, $\bar{n}^0$,$\mathbf{p^+}$,$\mathbf{p^-}$) and *hyperons*. *Hyperons* are the extremely unstable somewhat heavier particles and can be divided into four sub-groups, $\mathbf{\Lambda^0}$-particle (a neutral particle of mass about $\mathbf{180m_e}$), the Σ^- particles (Σ^-, Σ^0 and Σ^+ with masses in the range **2320** to $\mathbf{2340\ m_e}$), the Ξ-particles (Ξ^- and Ξ^0 with masses near $\mathbf{2580\ m_e}$) and **the** Ω^-particle (of mass about $\mathbf{3484\ m_e}$). There is no reason to doubt the existence of the *anti-particles* of these *fermions*. The total number of *baryons* the total number of *anti-baryons* is absolutely conserved in all interactions [4, 5, 6].

The *kaons, pions* and *eta meson* together with the *baryons* are placed into a group of strongly interacting particles, called *hadrons.*

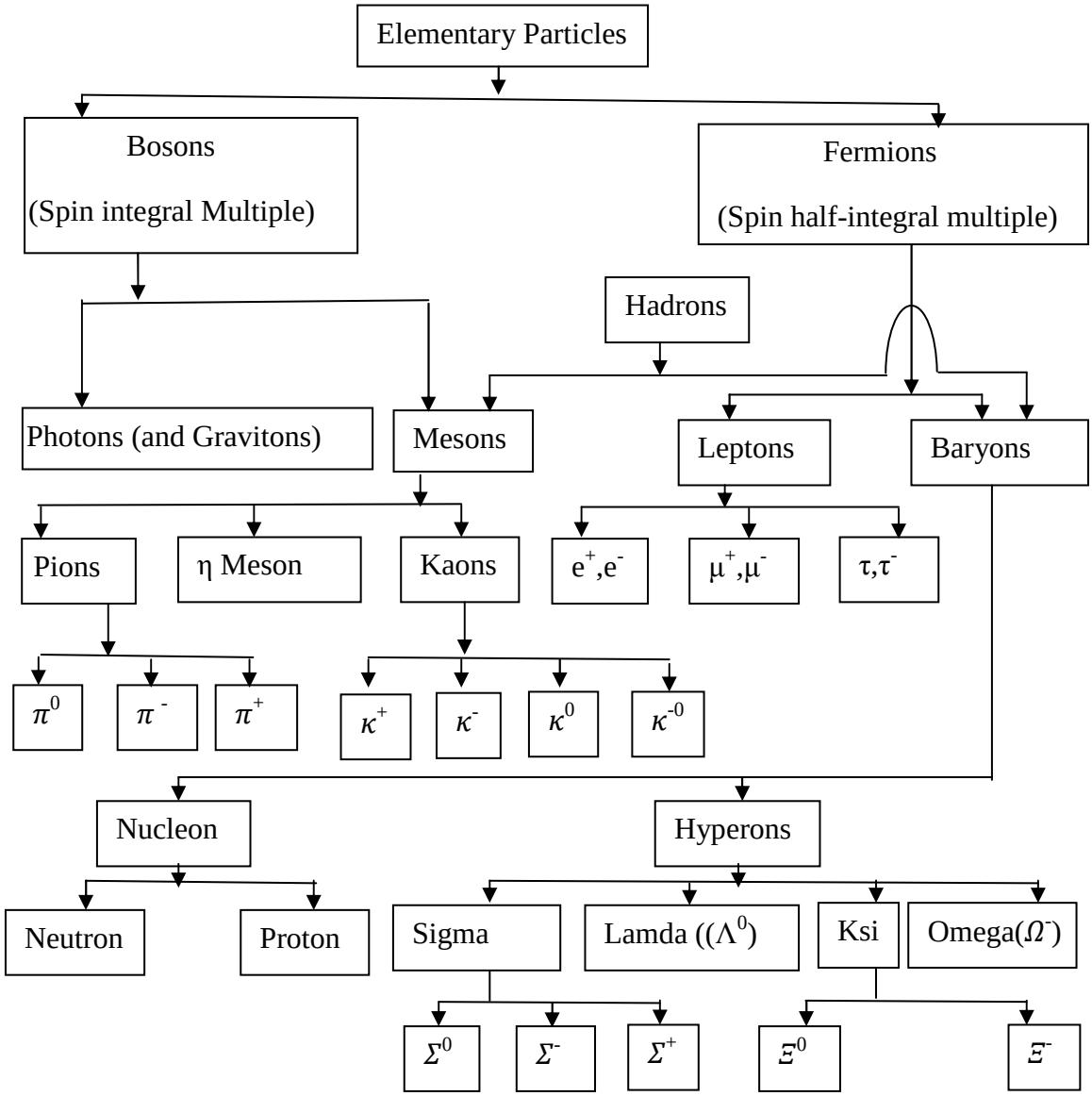

Figure 1.1: Classification of elementary particles

1.3 Particle interactions

The interactions among elementary particles can be classified into following four types:

1.3.1 Gravitational interaction

The first force that any of us discover is *gravity*. It holds the moon and earth together, keeping the planets in their solar orbits and binds stars to form our galaxy. Newton gave a formula $F=Gm_1m_2/r^2$ for the interaction between two masses. The gravitational effect does not depend on the color, size, charge, velocities, spin and angular orientation but depends on magnitude and inertia. The gravitational force between two nucleons separated by a nucleon diameter is

$$F=Gm_1m_2/r^2 \qquad (1.1)$$

$$= [6.7\times10^{-11}\ (1.7\times10^{-27})] / [(10^{-15})^2]$$

$$\approx 2\times10^{-34}\ \text{Newton}$$

and the gravitational attraction is only about $\mathbf{2\times10^{-49}}$ **joule**. Hence, we see that it plays no role in particle reactions. In the nineteenth century the forces were thought to be propagated by fields, space wrapped for particular effects. In the twentieth century these fields are explained in terms of agents or messengers, which actually propagate the effect. *Gravitation* can thus be explained in terms of the interactions of *gravitons*. Their mass must be zero and therefore, their velocity must be that of light. As the gravitational field is extremely weak, the gravitons can not be detected in laboratory.

1.3.2 Electromagnetic interaction

All of the ordinary chemical and biological effects are due to the interactions of electric charges and the fields they produce. The term *electromagnetism* is because the electricity and magnetism are both part of the same phenomenon. The appropriate law for the interaction of point charges bears the name of Coulomb ($F=q_1q_2/4\pi\varepsilon_0r^2$). For two protons 10^{-15} meter apart, the repulsion force will be $\mathbf{[9\times10^9\times\ (1.6\times10^{-19})^2/\ (10^{-15})^2]\approx230}$ **Newton**. It is about $\mathbf{10^{35}}$ times greater than the gravitational attraction

caused by the mass. The energy released by the complete separation of these protons would be **3×10^{-14} joules**.

If the particles are not at rest but are moving, the field will not only be an electric field but would be new one depending on the velocity and magnitude of the charge. When the charge accelerated, the energy radiates out in the form of electric and magnetic pulses. This energy comes from the agent that accelerates the charge. The pulse is called a *photon* and travels with the velocity of light. If the source charge is accelerating in an oscillating fashion, the propagated signal will consist of successive waves of electric and magnetic fields or the radio-photons. Thus, we see that the photons are emitted and reabsorbed by a charge. Interaction between two charged particles consists of an exchange of these photons. The strength of the electromagnetic interaction is given by the dimensionless fine structure constant **($\alpha = e^2/\varepsilon_0 \hbar c = 1/137$)**, and is due to photon exchanges.

The capture of photon can affect the production of *mesons* and *hyperons* by an electromagnetic interaction

$$\gamma + p \rightarrow \pi^0 + p$$

$$\gamma + p \rightarrow \Lambda^0 + K^+$$

An example of radiative capture reaction is

$$\pi^- + p \rightarrow n + \gamma$$

The neutral particles such as

$$\pi^0 \rightarrow \gamma + \gamma, \qquad \Sigma^0 \rightarrow \Lambda^0 + \gamma$$

$$\eta^0 \rightarrow \pi^+ + \pi^- + \pi^0, \qquad \eta \rightarrow \gamma + \gamma,$$

decay electromagnetically since these processes involve no change of *strangeness*. The decay processes such as $\Sigma^+ \rightarrow p^+ + \gamma$ are forbidden because the change $\Delta S = 1$ is required. The paradox that the decay of neutral particle is by electromagnetic indicator is resolved by introducing as an intermediate step in the overall reaction the virtual production of a ***nucleon, anti-nucleon***, (or electron-positron) pair. Thus, we have

$$\pi^0 \rightarrow (N+\bar{N}) \rightarrow \gamma + \gamma$$

The process of mutual annihilation of particles and anti-particles is an example of electromagnetic interaction.

1.3.3 Strong interaction

The strong nuclear interaction is independent of the electric charge. The force is same between **p-p** and **n-n**. For this purpose the proton and neutron are one but in different electric charge states. Strong interactions involve *mesons and baryons.* The range is very much shorter than that of *gravitational* or *electromagnetic interaction*. Strong interaction energy falls off rapidly when the distance between two particles increases. **Yukawa** in 1935 predicted the existence of heavy *quanta*, which played the same role in nuclear forces as *photons* in electromagnetic ones. From estimates of the range of nuclear forces, **Yukawa** predicted that the new particles, called *mesons*, should have the mass of the order of **200** to **300** electron masses [3]. The strength of the nuclear interaction is represented by the magnitude of the dimensional coupling constant $\mathbf{g^2/4\pi\hbar c \ (\approx 14)}$. It is about a thousand times the electromagnetic coupling constant $\boldsymbol{\alpha}$.

Strong interaction is responsible for *kaon* production; however; the decay of *mesons*, *nucleons* and *hyperons* proceeds by an electromagnetic or weak interactions.

1.3.4 Weak interaction

The *weak interaction* is responsible for the decay of *strange* and *non-strange particles* and for non-leptonic decays of strange particles. The numerical constant, which is characteristic of the weak interactions, is obtained from **Fermi's theory of β decay** [7]. Its value is $\mathbf{g_F = 1.41 \times 10^{-62}\ Jm^2}$. In analogy with the expression for the other interactions, the dimensionless weak interaction coupling constant is of magnitude

$$[g_F^2/(\hbar c)^2]\,[m_\pi c/\hbar]^4 \simeq \mathbf{5 \times 10^{-14}}.$$

Consider the reactions which do not involve a change of strangeness and yet which must be due to weak interaction. The neutron decay is the proto-type of all β-decays.

$$n \rightarrow p + e^{-} + \bar{\upsilon}_e$$

The nature of such an equation is that the reaction can go in either direction so long as energy is conserved and that any participant can be replaced on opposite side by its anti-particle, i.e. $p \rightarrow n + e^{+} + \upsilon_e$. Another variation of this four fermions interaction is the proton capture of an anti-neutrino ($\bar{\upsilon}_e + p \rightarrow n + e^{+}$).

In 1968, the electromagnetic force and the weak interaction were unified, when they were shown to be two aspects of a single force, now termed the electro-weak force. The theory of the weak interaction can be called **Quantum Flavordynamics** (QFD), in analogy with the terms QCD and QED, but in practice the term is rarely used because the weak force is best understood in terms of electro-weak theory (EWT)

1.4 The quark model

Murray Gell-Mann [8] and **G. Zweig** [9] proposed the quark model in 1964. This theory is based on the idea that the *hadrons* are build up from a limited number of "fundamental" units, which have acquired the name *quarks*. The original three *quarks* were labeled **u** (for up), **d** (for down) and **s** (for strange).

u quark has electric charge +2/3 e and strangeness 0.

d quark has electric charge – 1/3e and strangeness 0.

s quark has electric charge – 1/3e and strangeness -1.

Each quark has baryon number of B =1/3

Each *quark* has an *anti-quark* associated with it ($\bar{u}$, $\bar{d}$ and $\bar{s}$). The magnitude of each of the quantum numbers for the *anti-quarks* has the same magnitude as those for *quarks*, but the sign is changed [4].

1.5 Compositions of hadron according to quark model

Hadrons may be *baryons* or *mesons*. A baryon is made up of three quarks. For example, *proton* is made up of two **u** quarks and a **d** quark **(uud)**. For these quarks, the electric charges are +2/3, +2/3 and -1/3, for a total value of +1. The baryon

numbers are +1/3, +1/3 and +1/3 for a total of +1. The strangeness numbers are 0, 0 and 0 for a total strangeness of 0. All are in agreement with the quantum numbers for the proton. Fig below shows quark models of the *proton* and *antiproton, neutron* and *antineutron*. Electric charges is given in units of e.

Figure1.2: Quark combination of proton

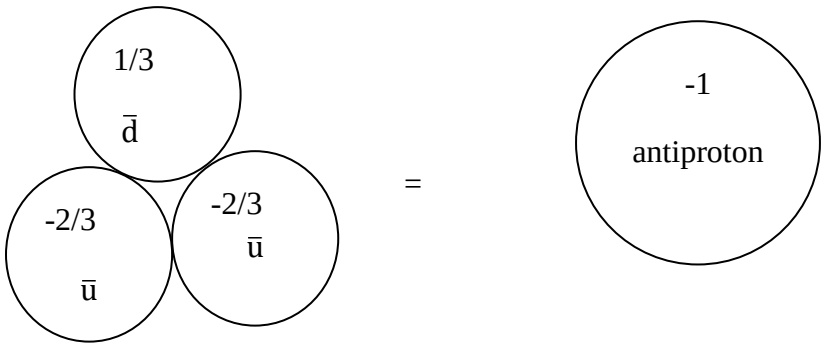

Figure 1.3: Quark combination of antiproton

A *meson* is made up of one *quark* and one *anti-quark*. For example, **the π^+** meson is the combination of a **u** quark and a **d** anti-quark **($u\bar{d}$).** Electric charges of these quarks are +2/3 and +1/3 for a total of +1. The *baryon* numbers are +1/3 and -1/3 for a total baryon number of 0. The *strangeness* numbers are 0 and 0 for a total of 0. All of these are in agreement with the quantum numbers for the **π-meson**. *Quarks* all have spins of ½, which accounts for the observed half-integral spins of *baryons* and 0 or 1 spins of *mesons*.

All known *hadrons* can be explained in terms of the various *quarks* and their *anti-quarks*. Table 1.1 shows the *quark* contents of five *hadrons* and how they account for the observed charges, spins and strangeness numbers of these particles.

Hadron	Quark content	Baryon Number	Charge	spin	strangeness
π^+	$u\bar{d}$	1/3-1/3=0	+2/3+1/3=+1	↑↓=0	0+0=0
K^+	$u\bar{s}$	1/3-1/3=0	+2/3+1/3=+1	↑↓=0	0+1=1
p^+	uud	1/3+1/3+1/3=+1	+2/3+2/3-1/3=+1	↑↑↓=1/2	0+0+0=0
n^0	ddu	1/3+1/3+1/3=+1	-1/3-1/3+2/3=0	↓↓↑=1/2	0+0+0=0
Ω^-	sss	1/3+1/3+1/3=+1	-1/3-1/3-1/3=-1	↑↑↑=3/2	-1-1-1=-3

Table 1.1: Compositions of some quarks according to quark model

1.6 Coloured quarks and gluons

There were problems with the quark model, one of them being Ω^- *hyperons*. It was believed to contain three identical **s** quarks **(sss)**. This violates the *Pauli Exclusion Principle* that prohibits two or more fermions from occupying identical quantum states. The proton, neutron and others with two identical quarks would violate this principle also. We can resolve this difficulty by assigning a new property to the *quarks*. We can regard this new property as an additional quantum number that can be used to label the three otherwise identical *quarks* in the $\boldsymbol{\Omega^-}$ If this additional quantum number can take any one of three possible values, we restore the *Pauli Principle* by giving each quark a different value of this new quantum number, which is known as colour. The three colours are *labeled red (R), blue (B), and green (G).* The Ω^- for example, would then $\mathbf{S_R S_B S_G}$. The *anti-quark* colours are *anti-red(R) anti-blue (B) and anti-green (G).*

An essential component of the quark model with *colours* is that all observed *meson* and *baryon* states are "*colourless*", i.e., either *colour anti-colour* combinations in the case of *mesons*, or equal mixtures of **R**, **B** and **G** in the case of *baryons*.

Since *hadrons* seem to be composed of *quarks*, the strong interaction between *hadrons* should ultimately be traceable to an interaction between *quarks*. The force between *quarks* can be modeled as an exchange force, mediated by the exchange of

massless spin -1 particles called *gluons*. Eight *gluons* have been postulated. The field that binds the *quarks* is a colour field. *Colour is to the strong interaction between quarks as electric charge is to the electromagnetic interaction between electrons*. It is the fundamental strong charge and is carried by the *gluons*. The *gluons* must therefore be represented as combinations of a *colour* and possibly a different *anti-colour*. The *gluons* are massless and carry their colour *anti- colour* properties just as other particles may carry electric charge. For example, Fig. 1.4 shows a gluon $\mathbf{R\bar{B}}$ being exchanged by *red* and *blue* quarks. In effect, the red *quark* emits its redness into a *gluon* and acquires blueness by also emitting *anti-blueness*. The *blue quark*, on the other hand, absorbs the $\mathbf{R\bar{B}}$ *gluon*, cancelling its blueness and acquiring a *red colour* in the process.

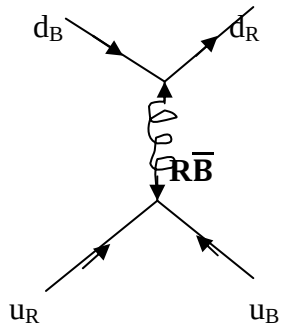

Figure 1.4: $R\bar{B}$ gluon

1.7 Charm, bottom and top

In 1970, **Glashow, Ilipoulis,** and **Maiani** proposed the existence of a fourth *quark*, called **c** or *charmed quark*. The *charmed quark* was suggested to explain the suppression of certain decay processes that are not observed. With only three *quarks*, the processes would proceed at measurable rates and should have been observed. The *charm quark* has a charge of 2/3e, strangeness 0 and a charm quantum number of +1. Other *quarks* have 0 *charm* [10].

In 1977, a new particle was discovered at **Fermi Lab** that provided evidence for yet another *quark*. This particle, called the *upsilon-meson*, was thought to be made up of the new quark called **b** (for bottom or beauty) along with the associated *anti-quark* $\mathbf{\bar{b}}$. **b** *quark* has electric charge -1/3 e.

Because *quarks* seem to come in pairs, it is expected that there is a partner to the **b** *quark*, called **t** (for top). It has a charge of +2/3 e.

1.8 Three generations of quarks and leptons

Both *leptons and quarks* appear to come in three generations of doublets, with all particles having spin 1/2. Table 1.2 and Table 1.3 show the properties of the three generations of *quarks* and *leptons* respectively. The first generation contains *two leptons*: *the electron and the electron neutrino,* and two quarks, *up and down*. All the properties of ordinary matter can be understood on the basis of these particles. The second generation includes *the muon* and *muon neutrino* and *the charm* and *strange quarks*. These particles are responsible for most of unstable particles and resonances created in high-energy collisions. The third generation includes *the tau* and *tau neutrino* and the *top* and *bottom* quarks.

Generation	Quark	Symbol	Charge	Strangeness	Charm
1	Up	u	+2/3	0	0
	Down	d	-1/3	0	0
2	Charm	c	+2/3	0	+1
	Strange	s	-1/3	-1	0
3	Top	t	+2/3	0	0
	Bottom	b	-1/3	0	0

Table 1.2: Properties of the Three Generations of Quarks

Generation	Lepton	Symbol	Charge
1	electron	e^-	-1
	e-neutrino	υ_e	0
2	muon	μ^-	-1
	μ-neutrino	υ_μ	0
3	tau	τ^-	-1
	τ-neutrino	υ_τ	0

Table 1.3: Properties of the Three Generations of Leptons

1.9 Particle codes

In hadronic interaction different particles have their **GEANT** code. Some of them are given below in Table 1.4.

GEANT Code	Particle	GEANT Code	Particle
1	γ	25	$\bar{n}$
2	e^+	26	$\bar{\Lambda}$
3	e^-	27	$\bar{\Sigma}^-$
4	N	28	$\bar{\Sigma}^{-0}$
5	μ^+	29	$\bar{\Sigma}^{\pm}$
6	μ^-	30	Ξ^{0-}
7	π^0	31	$\Xi^{\pm}$
8	π^+	32	$\Omega^{\pm}$
9	π^-	33	$\dagger^+$
10	K^0_L	34	$\dagger^-$
11	K^+	35	D^+
12	K^-	36	D^-
13	N	37	D^0
14	P	38	$\bar{D}^{-0}$
15	$\bar{p}$	39	D_s^+
16	K^0_S	40	Ds^+
17	η	41	Λc^+
18	Λ	42	W^+

19	$\sum^{+}$	43	W^{-}
20	$\sum^{o}$	44	Z^{0}
21	$\sum^{-}$	45	D
22	Ξ^{o}	46	T
23	Ξ^{-}	47	α
24	Ω^{-}	48	Gν

Table 1.4: Particle codes [11]

CHAPTER TWO

Eta meson photoproduction

The eta (η) meson made of a mixture of *up*, *down* and *strange quarks* and their *anti-quarks*. The η is a pseudo scalar meson.

Composition of η = $\frac{u\bar{u}- d\bar{d}-2\, s\bar{s}}{\sqrt{6}}$ where **u**, **d** and **s** are *up, down* and *strange* quarks and $\bar{\mathbf{u}}$, $\bar{\mathbf{d}}$ and $\bar{\mathbf{s}}$ are *anti-up, anti-down* and *anti-strange* quarks respectively

2.1 Properties of η meson

Properties of eta meson are shown in Table 2.1 below.

Property	Value
Mass	(547.51 ± 0.18)MeV
Valence Quarks	$(u\bar{u} + d\bar{d} - 2s\bar{s}/\sqrt{6})$
Lifetime	$<10^{-18}$ s
Charge (Q)	0
Isospin (I)	0
Orbital Angular Momentum (L)	0
Total Angular Momentum (J)	0
Strangeness (S)	0
Parity (P)	-
Charge Conjugation (C)	+

Table 2.1: Properties of the η meson [12]

2.2 Decay mode

The proton can be excited using photons with energies **Eγ ≥ 702MeV**, producing the reaction:

$$\gamma p \rightarrow \eta p \quad (2.1)$$

η meson, having lifetime of $\mathbf{<10^{-18}\ s}$, decay before detection. Of the various decays of the η, 72% occur via the following neutral modes:

$$\eta \rightarrow 2\gamma \quad (2.2)$$

$$\eta \rightarrow 3\pi^0 \rightarrow 6\gamma \quad (2.3)$$

with branching ratios of (**39.39 ± 0.24**)% and (**32.52 ± 0.26**)% respectively[12]. The main aim of this thesis work is to study photoproduction reaction γp → ηp → γγp.

2.3 Kinematics for γp → ηp

In our experiment, liquid hydrogen was used as the target. After the interaction of the incident photon beam with the proton, the outgoing η makes a polar angle θ with respect to the direction of the incident photon.

Let us consider $\boldsymbol{P^{\mu}_{beam}}$,$\boldsymbol{P^{\mu}_{target}}$, $\boldsymbol{P^{\mu}_{\eta}}$ and $\boldsymbol{P^{\mu}_{p}}$ and as the four-momenta of the *incident photon, target proton, η meson* and *product proton* respectively. Now, using the energy-momentum conservation relation in four-momentum notation, we may write

$$\boldsymbol{P^{\mu}_{beam} + P^{\mu}_{target} = P^{\mu}_{\eta} + P^{\mu}_{p}} \quad (2.4)$$

The superscript letter μ takes four values $\mu = 0,1,2,3$, where $\mu = 0$ gives the energy (E) and the other values of μ represent the three-momentum ($P = P^1, P^2, P^3$) of the four vector ($\mathbf{P^{\mu}}$). The four-momentum of **η** is determined by summing the four-momenta of its photon decays (2γs) as

$$\boldsymbol{P^{\mu}_{\eta}} = \sum_{i}^{2} \mathbf{P^{\mu}_{\gamma_i}} \quad (2.5)$$

In the laboratory frame, these four-momenta can be expressed as

$$\boldsymbol{P^{\mu}_{beam}} = (E_{beam}, P_{beam}), \quad (2.6a)$$

$$\boldsymbol{P^{\mu}_{target}} = (E_{target}, P_{target}) = (M_{target}, 0) \quad (2.6b)$$

$$\boldsymbol{P^{\mu}_{\eta}} = (E_{\eta}, P_{\eta}) \quad (2.6c)$$

Since the square of the target four-momentum gives the invariant mass of the target (M_{target}), we can write $\mathbf{P^2_{target}} = \mathbf{P^{\mu}_{target}}.\mathbf{P_{target\mu}} = E^2_{target} - P^2_{target} = M^2_{target}$. As the target is at rest in the laboratory frame, it follows that $P_{target} = 0$ and $E_{target} = M_{target}$. The photon energy E_{beam} is measured by using the *Glasgow Photon Tagger* and $E_{beam} = P_{beam}$ in Eq. (2.6a). When there is only one undetected particle in the final state (like proton here), its kinematics is reconstructed by using four-momentum conservation. Using Equations (2.4) and (2.6c), the four-momentum P_p^{μ} of the undetected proton can be expressed as

$$\boldsymbol{P^{\mu}_{p}} = \boldsymbol{P^{\mu}_{beam}} + \boldsymbol{P^{\mu}_{target}} - \boldsymbol{P^{\mu}_{\eta}}$$

$$\boldsymbol{P^{\mu}_{p}} = \boldsymbol{P^{\mu}_{beam}} + \boldsymbol{P^{\mu}_{target}} - \sum_{\mathbf{i}}^{\mathbf{2}} \mathbf{P^{\mu}_{\gamma_i}} \qquad (2.7a)$$

Using equation (2.6a) and (2.7a)

$$E_p = E_{beam} + M_{target} - \sum_i^2 E_{\gamma_i}, \qquad (2.7b)$$

$$P_p = P_{beam} - \sum_i^2 P\gamma i \qquad (2.7c)$$

Thus the missing mass MM (η) of η is given as

$$MM\ (\eta) = M_p = \sqrt{(E_p^2 - P_p^2)} \qquad (2.8)$$

The outgoing η makes a polar angle θ with respect to the direction of the incident photon [13].

2.3.1 Event selection

The *eta* meson has a very short lifetime, so only the photons resulting from their decay are determined $\eta \rightarrow 2\gamma$. When a particle decays, its momentum four-vector is conserved. Consequently, the momentum four-vector of an *eta* meson is equal to the sum of the momentum four-vectors of the photons resulting from its decay. For our research work of $\gamma p \rightarrow \eta p \rightarrow 2\gamma p$, we considered two photons and a proton in the final state.

2.3.2 Particle identification in $\gamma p \rightarrow \eta p \rightarrow \gamma\gamma p$

As we have seen, the final state, we detected two photons and a proton. As we know that lifetime of η mesons is very small, so only the photons resulting from their decays $\eta \rightarrow 2\gamma$ were detected. The momentum four-vector of a η is equal to the sum

of the momentum four-vectors of the two photons resulting from its decay. The η events were identified by constructing the invariant mass of the two photons.

For the reaction $\gamma p \rightarrow \eta p \rightarrow \gamma\gamma p$ all information about the initial state was available: the energy of the incident photon beam and its direction (along the beam axis), and the target nucleon, which was assumed to be at rest. The momentum four-vector of the η (the four-vector of the two decay photons) was also known. Thus, using the principal of conservation of energy and Momentum, the four-vector of the η as the missing particle is given by

$$\boldsymbol{P_{\eta}^{\mu}} = \mathbf{P_{beam}^{\mu}} + \mathbf{P_{target}^{\mu}} - \Sigma_{i}^{2}\,\mathbf{P_{\gamma_i}^{\mu}}$$

where $\mathbf{P_{beam}^{\mu}}$ and $\mathbf{P_{target}^{\mu}}$ are the corresponding momentum four-vectors of the incident photon and target nucleon, respectively. For the target nucleon, we assumed $\mathbf{P_{target}^{\mu}} = (Mp, 0)$, where Mp is the proton mass [12, 13].

2.3.3 Identification of a proton by missing mass

In the reaction $\gamma p \rightarrow \eta p \rightarrow \gamma\gamma p$ the proton is an undetected particle; however, it can be reconstructed. As the momentum four-vectors of the incoming photon beam, the target proton, and the two final-state photons are known, the four-momentum of the missing proton is given by

$$\mathbf{P_{proton}^{\mu}} = \mathbf{P_{beam}^{\mu}} + \mathbf{P_{target}^{\mu}} - \Sigma_{i}^{2}\,\mathbf{P_{\gamma_i}^{\mu}}$$

The missing mass-squared of the two photons in the final state $(MM_{2\gamma})^2$ is obtained by squaring the four-vector $\mathbf{P_{proton}}$ as

$$(MM_{2\gamma})^2 = (\mathbf{P_{proton}^{\mu}})^2$$

so missing mass of two photons provides proton mass [14].

2.4 Threshold energy expression

The minimum energy of photon required to produce *eta meson* is called threshold energy of *eta meson*. Consider a beam of photon strikes liquid hydrogen target at rest and product particles are *eta* meson and photon. So our reaction becomes

$$\gamma p \rightarrow \eta p$$

Then from conservation of momentum, initial momentum of the reactant is equal to the final momentum of the product. So we can write

$$(\mathbf{P}^{\mu}_{\mathbf{beam}} + \mathbf{P}^{\mu}_{\mathbf{target}})^2 = (\boldsymbol{P}^{\mu}_{\eta} + \boldsymbol{P}^{\mu}_{p})^2$$

where $\mathbf{P}^{\mu}_{\mathbf{beam}}$, $\mathbf{P}^{\mu}_{\mathbf{target}}$, $\boldsymbol{P}^{\mu}_{\eta}$ and $\boldsymbol{P}^{\mu}_{p}$ represents four-momentum of striking photon, four-momentum of target, four- momentum of η and four-momentum of proton, respectively.

$$(E_\gamma + E_p)^2 - (P_\gamma + P_p)^2 = (E_\eta + E_p)^2 - (P_\eta + P_p)^2$$

But momentum of eta and proton is zero. i.e. $P_\eta = P_p = 0$ **,** $E_p = m_p$ and $E_\eta = m_\eta$

$$E_\gamma^2 + 2E_\gamma m_p + m_p^2 - P_\gamma^2 = m_\eta^2 + m_p^2 + 2m_p m_\eta$$

$$E_\gamma^2 - P_\gamma^2 + 2E_\gamma m_p = m_\eta^2 + 2m_p m_\eta$$

$E_\gamma^2 - P_\gamma^2 = 0$, because real photon has no mass and its momentum and energy are same [15].

which gives $(E_\gamma)_{\text{threshold}} = \dfrac{m_\eta^2 + 2m_p m_\eta}{2m_p}$ for the reaction $\gamma p \rightarrow \eta p$ (5.1)

For the reaction $\gamma p \rightarrow \eta p$,

$\mathbf{m_\eta}$ **=550.095 MeV**

$\mathbf{m_p}$**=938.27 MeV**

then Eqn. (6.1) gives **,**(E_γ)threshold = **702.77 MeV**

This is the minimum energy of photon beam required to produce η meson. Therefore, for our reaction $\gamma p \rightarrow \eta p$ we have to provide energy of photon more than threshold energy. For this purpose, we prepared different *dat* files with energy of incident photon more than threshold energy. Detail discussion of *eta* photoproduction is given in chapter 6.

CHAPTER THREE

Review of photoreaction γp → ηp

Over the last several years, there has been increasing number of work in the photoproduction of *eta mesons* with *protons, pions and electrons* and their interactions with *nucleons* and *nuclei*. One of the first *eta meson* nuclear experiments performed at **SATURNE** [16] in 1988, reported surprisingly large *eta meson* production rates near threshold in the reaction $p(d_3, He)\eta$. The large cross sections permitted not only a more precise determination of the eta mass [17] but also were used to perform rare decay measurements of the *eta mesons* [18]. Additional experiments involving pion induced *eta* production performed at **Los Alamos** [19]. Again the experimental cross section at threshold region of the reaction ^{3}**He** (π, η) $^{3}_{H}$ are above the theoretical calculations [20].

The advent of high duty cycle electron accelerators opens for the first time the opportunity to study the reactions **N (γ, η) N** and **N (e, e´η) N** in detail. Our present knowledge of the *(γ, η)* process is based solely on some old measurements around 20 years ago, along with very few more recent data from Bates [21] and Tokyo [22]. Over the last two years eta production from the nucleon has been measured at **Mainz** and **Bonn** with an accuracy of more than an order of magnitude better than in older experiments. At Mainz, the **TAPS** collaboration has obtained high quality data for angular distributions and total cross sections for photon energies between **threshold** and **790 MeV** both on the nucleon and on nuclear targets ^{12}C, ^{40}Ca. That may be considered to be a qualitative breakthrough in the experimental field [23].

In this work, we have presented a study of photoproduction of eta meson i.e.

$$\gamma p \rightarrow S_{11}(1535) \rightarrow \eta p$$

at **MAMI** (Mainz Microtron): (see chapter 4.1)**.** This study is helpful for the determination of tagging efficiency, nuclear cross section, further study of production

process and the final state interactions without being obscured by the details of the nuclear transition densities.

William A. **McNeely** carried out eta photoproduction with hydrogen target, at 0˚ and 180˚ for the energy between 0.7 and 1.1GeV**,** experimentally in 1971. Similarly, *Eta(547)* and *Eta(958)* meson photoproduction on the proton was carried out by **Michael Dugger** in 2001[24]. In the same way measurement of the branching ratio for eta-meson decay into a neutral pion and two photons, was carried out by **Jason William Brudvik** in 2007 [20]. Eilidh Fiona MCNicoll did later Eta photoproduction study with the upgraded Glasgow tagger at MAMI from University of Glasgow, Scotland on January 2010 [12]. The next two sub-sections describe these studies.

3.1 Work and result carried out by Jason William Brudvik

This dissertation presents the results of a measurement of the branching ratio for the rare decay $\eta \rightarrow \pi^0\gamma\gamma$. The experiment was carried out in the A2 hall of the Mainz Microtron facility at the *Institut für Kernphysik*, on the campus of *Johannes Gutenberg Universität Mainz*, in Mainz, Germany. The experiment used the *Glasgow-Mainz Tagger*, which is a recoil-electron spectrometer, to determine the energy of the incident photons. The principal detector is the *Crystal Ball*, a highly segmented multiphoton spectrometer surrounding the experimental target (see chapter 4). There is also a *forward detector*, *TAPS*, which is a *multiphoton spectrometer* arranged as a downstream wall of detectors. Furthermore, setup included an instrument used to differentiate between charged and neutral particles called the Particle Identification Detector, and a liquid hydrogen target. The kinematic technique was used to select the $\eta \rightarrow \pi^0\gamma\gamma$ events. The major backgrounds, namely $\eta \rightarrow 3\pi^0$and decay $\eta \rightarrow \gamma\gamma$ and $2\pi^0$ production were measured simultaneously. The result for the branching ratio is BR ($\eta \rightarrow \pi^0\gamma\gamma$) = $(\mathbf{2.0\pm0.7}) \times \mathbf{10}^{-4}$. However, we simply study photoproduction of *eta* meson.

In this thesis, he has used some histograms by using Monte Carlo methods. From the result of Jason's dissertation which are also helpful for our study of γp → ηp → γγp are shown in Fig. 3.1. The figure shows invariant mass spectrum of η for η → 2γ and η → 6γ decay. The peak value of mass invariant curve is approximately **547 MeV** which is the mass of *eta meson*.

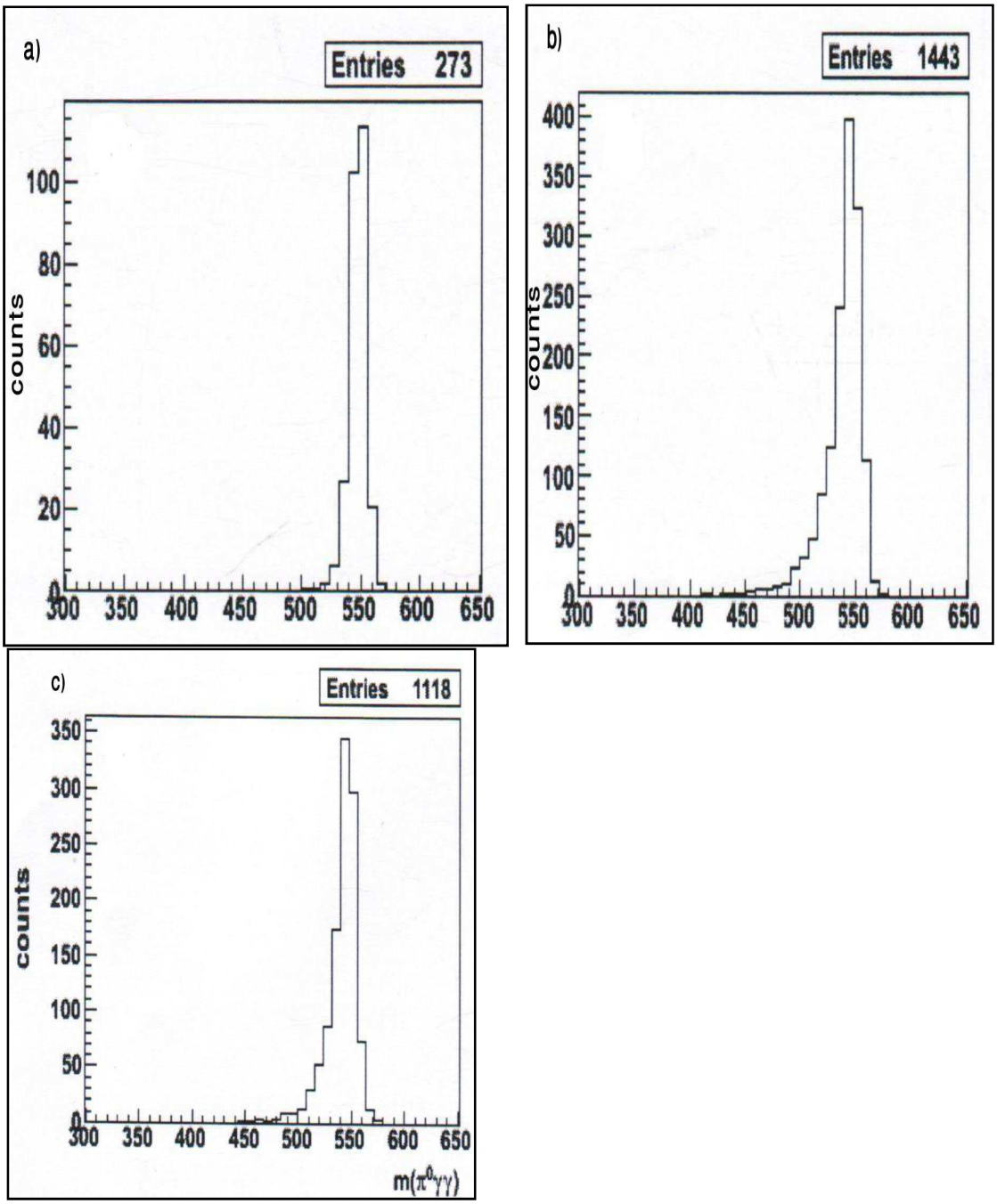

Figure 3.1: The invariant mass spectrum of a) η→ π0γγ b) η→3π0 c) η → γγ [24]

3.2 Work and result carried out by Eilidh Fiona MCNicoll

MCNicoll presented differential cross-section measurements for η photoproduction on the proton:

$$\gamma p \rightarrow \eta p$$

in the energy range **$707 \leq E\gamma \leq 1403$MeV** over the full polar angular range,$0^{\circ} \leq \theta^{*}\eta \leq 180^{\circ}$. The two dominant η decay channels:

$$\eta \rightarrow 2\gamma \text{ and } \eta \rightarrow 3\pi^{0} \rightarrow 6\gamma$$

had been analysed separately. A comparison of results from these final states was given. Data were also compared to the **SAID** model and to recent experimental results from the **GRAAL** collaboration. Through this comparison, evaluation was made of the tagger upgrade.

Differential cross-sections from **threshold** to **1100MeV** are shown in figure 2.3 [12].

From the η photoproduction threshold at **E_{γ} = 707MeV** to **890MeV**, the angular distribution of the differential cross-section is quite flat, indicating the dominance of s-wave processes in the reaction mechanism, in this case the $S_{11}(1535)$. The resonant shape is truncated at threshold and rises to a maximum at **E_{γ} = 805MeV**, corresponding to the centre-of-mass energy of **1535 MeV**. This accounts for the cross-section being highest in this energy range. From **918** to **1024MeV**, the differential cross-sections rise to a maximum. By **1050MeV**, this maximum has become more pronounced and moved to a forward angle. In Fig. 2.2 the triangles, present standard error associated with the measurement of the variation of differential cross section for $\gamma p \rightarrow \eta p$ analysis.

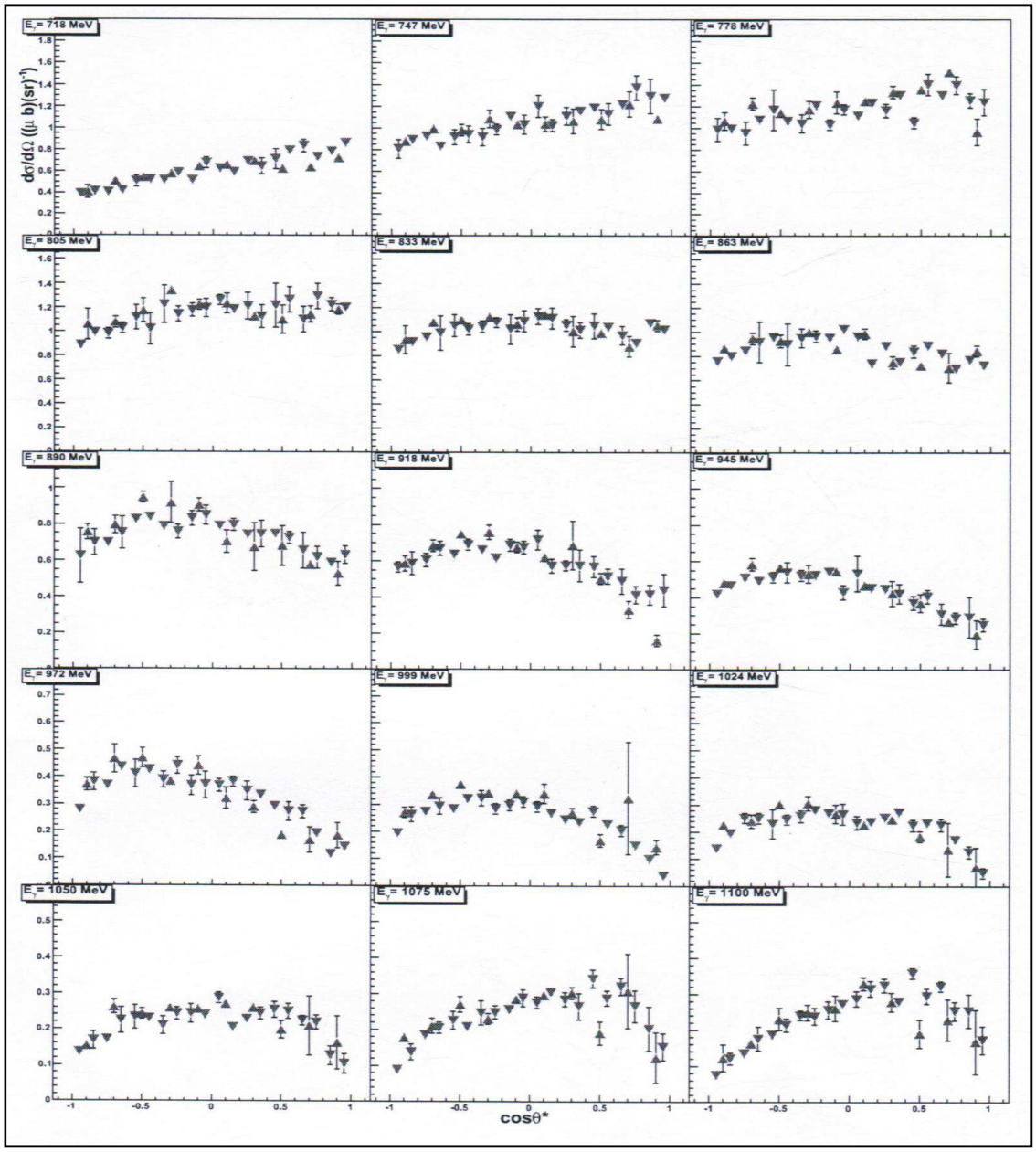

*Figure 3.4: Differential cross section as a function of cosθ*η for E_γ in the range 1124 to 1395 MeV, with symbols as defined in figure 2.3[12]*

In this dissertation, we have not presented the cross section measurement of our photoproduction reaction γp → ηp, as we are not analysing for the real data.

CHAPTER FOUR

Experimental setup

This chapter describes the experimental facility used by the *A2 Collaboration in Mainz, Germany.* The set-up is mainly comprised of the three components shown in Fig. 4.1. The primary component is the electron accelerator, which is also called the Mainz *Microtron (MAMI-C).* It produces a continuous-wave electron beam. The beam of electrons from *MAMI-C* is directed onto a thin diamond or copper foil generating a beam of high-energy photons via a bremsstrahlung process. The second component is the *Glasgow Photon Tagging Spectrometer*, which is used to analyze the momentum of the corresponding bremsstrahlung electrons. The photon beam is allowed to impinge on a target causing the production of various particles. The third component, which is the detector system used to detect these particles and their decays, consists of the *Crystal Ball (CB) and the TAPS spectrometer***.**

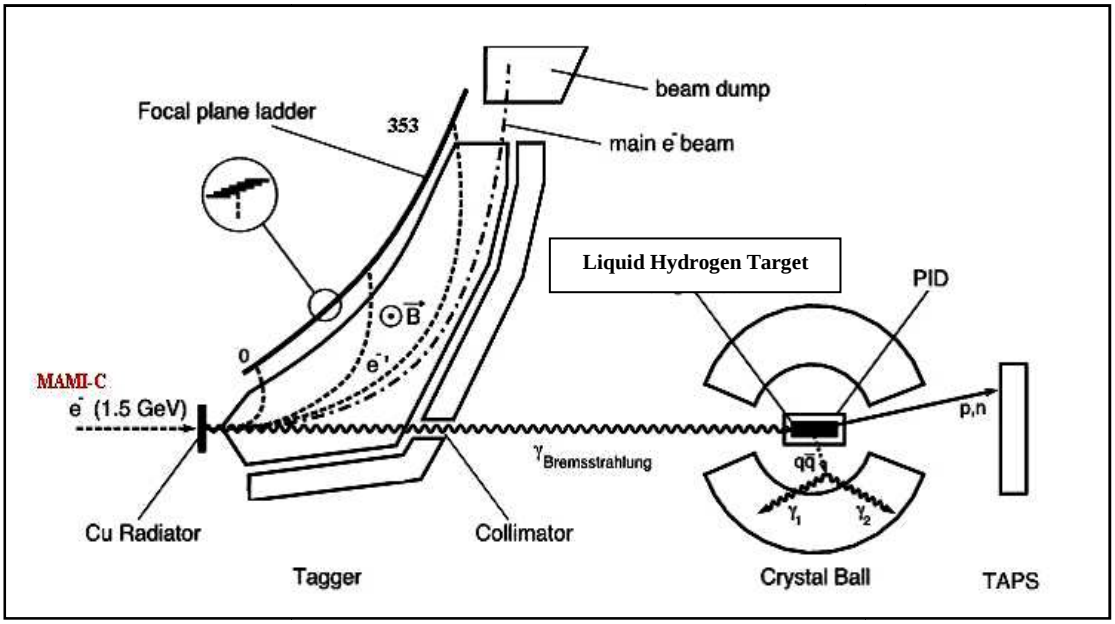

Figure 4.1: The experimental set-up in the A2 Hall in Mainz consists of three main components: (i) MAMI electron accelerator for production of electrons up to 1.5 GeV, (ii) Glasgow Photon Tagger,(iii) Detector system (CB, TAPS, PID, MWPC)

4.1 Mainz Microtron (MAMI)

The *Mainz Microtron (MAM*I) is an intense, stable and continuous-wave accelerator that accelerates electrons to the relativistic limit. It is operated by the Institute f¨ur Kernphysik at Johannes *Guttenberg University at in Mainz, Germany*. The accelerator in its current configuration was constructed in four stages: (i) *MAMI-A1, (ii) MAMI-A2, (iii) MAMI-B, and (iv) MAMI-C. MAMI-A1* was installed in 1979, producing electrons up to **14 MeV**. In 1983, a second microtron was added, upgrading the facility to *MAMI-A2* with maximum energy **183 MeV**. With the addition of a third microtron in 1990, the maximum energy was increased to **855 MeV** under the name *MAMI-B. MAMI-C,* which is the present facility, was set into operation in December, 2006 producing a continuous high quality electron beam with maximum energy **1.5 GeV**. It supplies the electron beam to any of the experimental halls *(A1, A2, A4, X1*) as shown in Fig. 4.2.

MAMI-C consists of three cascades of *RTMs (Race Track Microtrons)* and a recently added *Harmonic Double-Sided Microtron (HDSM).* This new *HDSM* is considered as a worldwide unique recirculation electron accelerator. It consists of two systematic pairs of 90˚-dipoles, each forming an achromatic 180˚ bending system as shown in Fig. 4.3. In order to compensate for the strong vertical defocusing due to the 45˚-pole face inclination at beam entrance and exit, these dipoles incorporate an appropriate field gradient normal to the pole edge. This functions as a scheme for transversal focusing, with only two quadrupole doublets on each of the two dispersion-free anti-parallel linac axes. In the *HDSM*, the two linacs operate at different frequencies: one at **2.45 GHz** and the other at **4.90 GHz**. The linac operating at the lower frequency maintains a higher longitudinal stability. The linac at the higher frequency is responsible for a synchronous acceleration energy gain per turn below **20 MeV** [22]. For the *HDSM*, the electron energy gained per turn is given by

$$\Delta E/\text{turn} = \frac{n \times ecB}{(\pi - 2) \times \lambda_{rf}} \qquad (4.1)$$

where n is the number of complete turns made by electrons (n = 1 is the lowest possible value) and λ_{rf} is the rf-wavelength. The injection of the electrons is made from the result of RTM3 (MAMI-B).

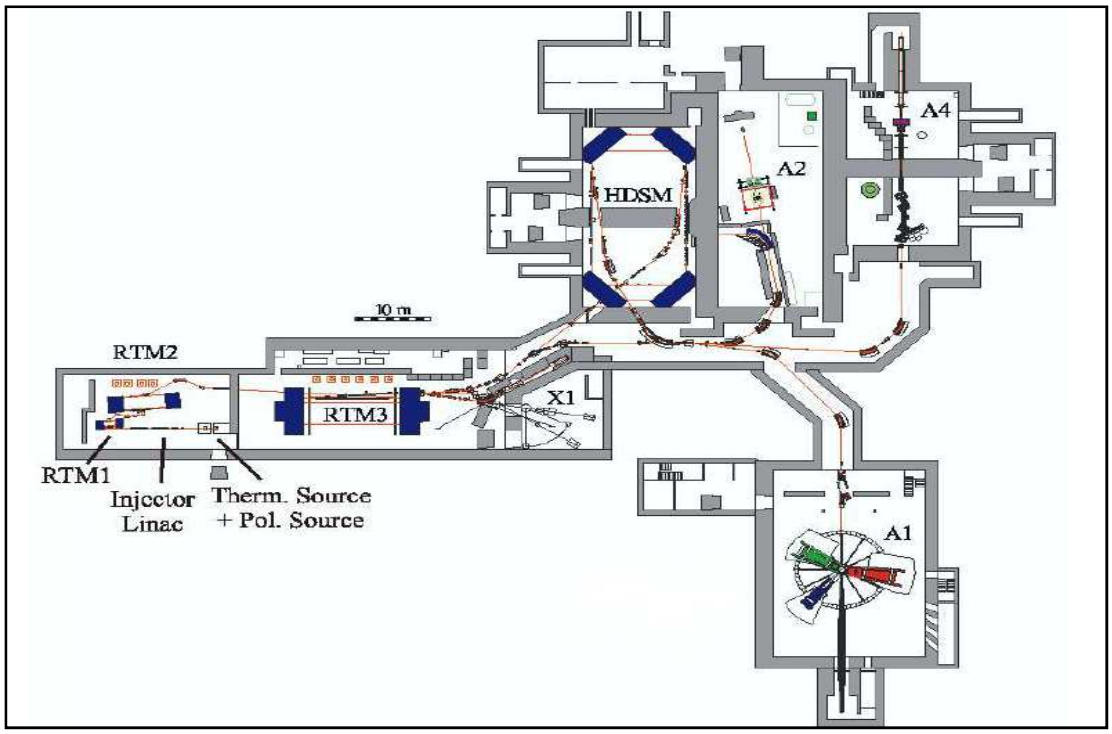

Figure 4.2: The floor plan of MAMI facility. Three racetrack microtrons RTM1, RTM2, and RTM3 together with the Harmonic Double Sided Microtron (HDSM) produce an electron beam with energy up to 1508 MeV in MAMI-C. A1, A2, A4, and X1 are the experimental halls. Our experimental work was carried out in the A2 Hall

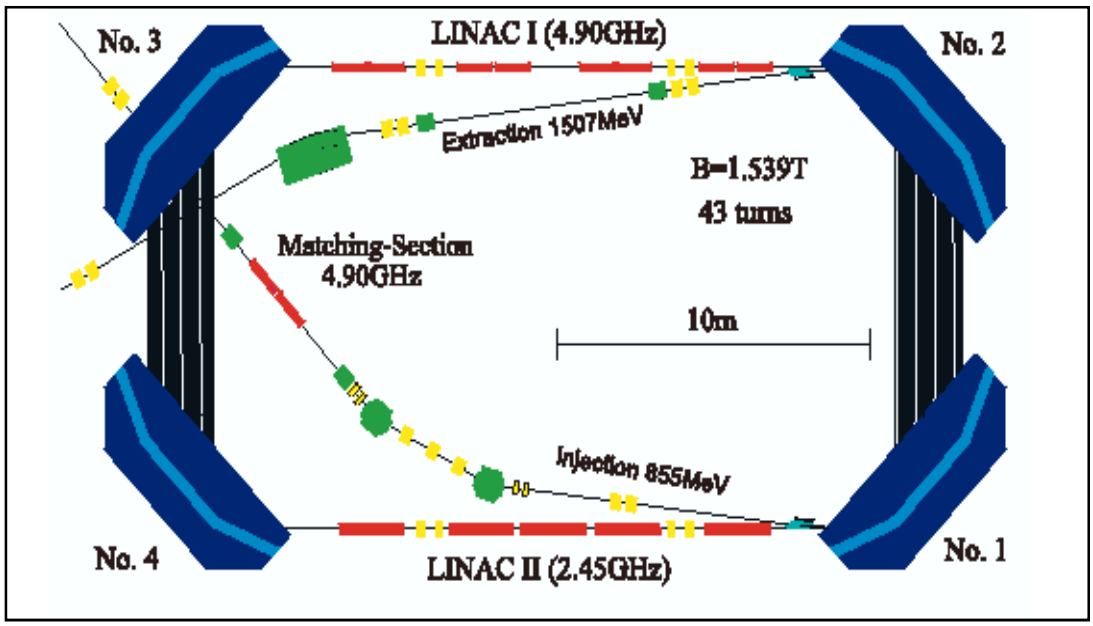

Figure 4.3: General layout of the HDSM. HDSM consists mainly of two pairs of 90◦ bending magnets and two linear accelerators. These two linear accelerators work on two different frequencies, 2.45 GHz and 4.90 GHz [26].

with the value of B = 1.23 T, λ_{rf} = 0.1224 m; thus, from Eq. (4.1), ΔE = 41.1 MeV/turn. This also needs 20 m long linacs, which would not fit into the existing MAMI-floor, as shown in Fig.4.2. Moreover, it would consume four times the electric power of MAMI-B. So it is practicable to adjust the frequency of the *HDSM* at **4.90 GHz** (λ_{rf} = 0.0612 m) with a small variation in B value as **1.823 T**, to keep the length of the linacs about 10 m and the other parameters similar to that of *RTM3.* The *HDSM* takes the beam energy from **855 MeV** to **1508 MeV** by **43** turns in **14.0 to 16.7 MeV** per step through its accelerating section.

4.2 The Crystal Ball

The *Crystal Ball (CB)* was designed in 1974 as a multiphoton spectrometer with high detection efficiency over a large solid angle. It was initially used to detect photons produced in high-energy e−e+ collisions [27] at *SLAC (Stanford Linear Accelerator Center in Stanford, CA).* From 1978 to 1981, it was used to investigate the spectroscopy of the J/Ψ and radioactive decays of particles such as τ , Ψ, and D at SPEAR. After this period, it was put into storage at *SLAC* until 1995 when it was moved to the AGS facility at *BNL,* where it was used for the study of nucleon and hyperons spectroscopy, and rare η decays. It was moved to Mainz in 2002 and after completion of a major upgrade of the detector's electronics it was used at *MAMI-B* until 2005. It resumed operation in 2007 as the central detector at *MAMI-C.*

The *CB* consists of **672** thallium-doped sodium iodide *NaI (Tl)* crystals. These crystals are optically isolated from one another by wrapping them in reflecting paper and aluminized mylar. A *SRC L50B01* type photomultiplier tube *(PMT)* of **5.1 cm** diameter and **21 cm** in length is arranged behind each crystal to convert the resulting light pulse into electric signals. Each crystal is shaped like a truncated pyramid of length **40.6 cm** (or 15.7 radiation lengths) with the side of inner face **5.1cm** in length and the side of outer face **12.7 cm** as shown in Fig. 4.4. These crystals are arranged to form a ball structure as shown in Fig. 4.5 with an inner radius of **25.3 cm** and outer radius of **66cm**.

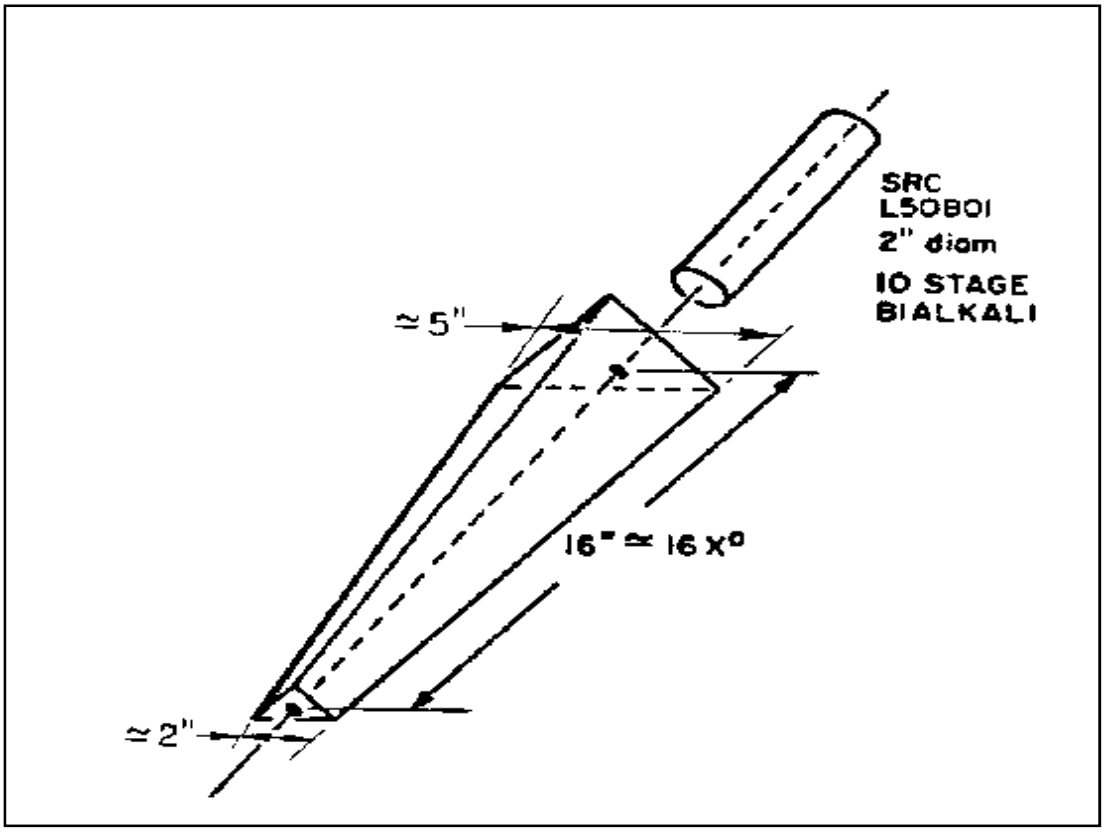

Figure 4.4: An individual crystal in the CB is 40.6 cm long with a truncated pyramid shape

The geometry of the *Crystal Ball* is that of an *icosahedron* (a solid with 20 faces). These **20** faces form "major triangles" which in turn are divided into faces of four "minor triangles" each containing nine crystals as shown in Fig. 4.6. When these crystals are stacked together closely they form a spherical shell of **720** elements. In order to make a space for the photon beam and the target system, **24** crystals were removed from the opposite poles. The *CB* is divided into two hemispheres: an upper one and a lower one separated with two **0.8 mm** stainless steel plates and a **0.8 cm** air gap. Because of this, an active space amounting to **1.6%** of the solid angle (or 4π) is introduced. Since *NaI(Tl)* is hygroscopic, all the crystals are hermetically sealed in the two separated hemispheres. This also helps to control the temperature **(23 ± 2˚ C),** pressure (low) and humidity **(~30%)** inside the hemispheres.

In the *Crystal Ball*, the incident photon beam produces electromagnetic showers that in turn deposit their energy in the *NaI(Tl)* crystals depending on the energy of the photon. An incident photon below **10 MeV** may deposit energy only in one or two crystals whereas a photon up to **400 MeV** deposits **98%** of its energy in a

cluster of **13** crystals. Because of this, the measurement of photon energy from the *Crystal Ball* is considered quite precise and the energy resolution is taken as

$$\frac{\sigma E}{E} = \frac{2.05\%}{E(GeV)0.36} \qquad (4.2)$$

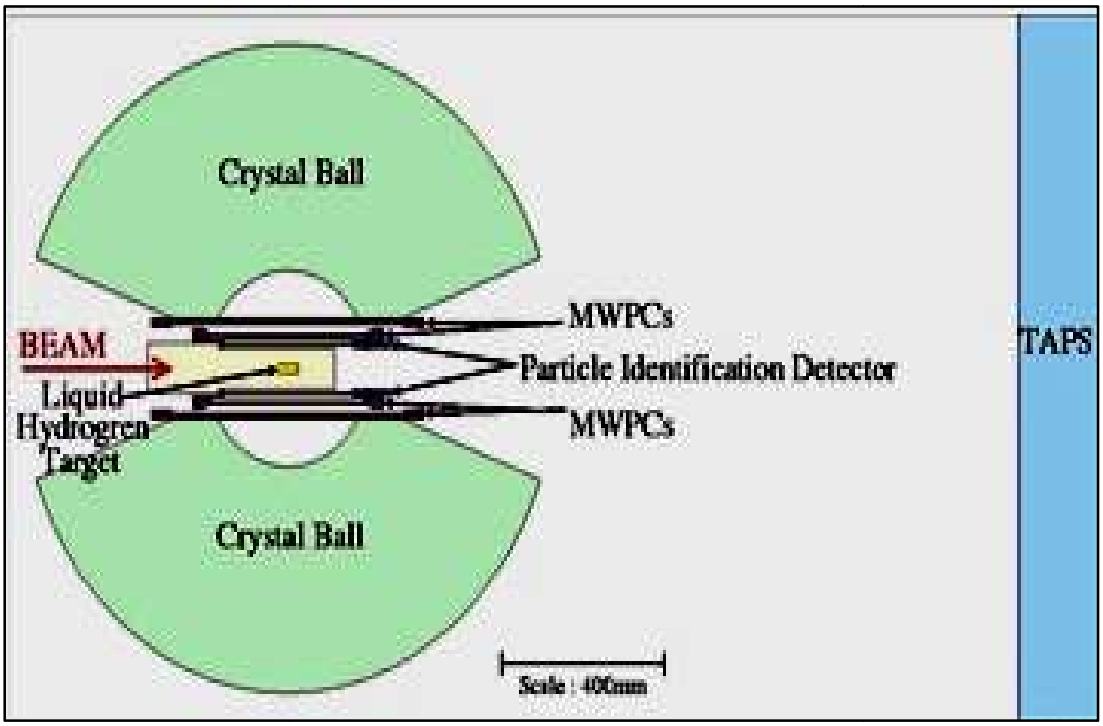

Figure 4.5: A transverse view of the Crystal Ball showing the sub detectors inside it. A liquid hydrogen target is also located at its center.

Because of the high granularity of the *Crystal Ball* it also has a good position resolution. For hadrons and charged particles, the positional resolution is not optimal as the hadronic shower has less transverse extension. Thus for charged particles other additional detectors are required. Some of the important properties of the *Crystal Ball* are listed in Table 4.1[23, 24, 25].

Azimuthal angular acceptance	$0^{\circ} \leq \varphi \leq 360^{\circ}$
Polar angular acceptance	$20^{\circ} \leq \theta \leq 160^{\circ}$
Azimuthal Angular resonance (σ_{θ})	$(2 - 3^{\circ})/\sin\theta$
Polar angular resolution (σ_{φ})	$2 - 3^{\circ}$
Photon Energy Resolution (σ_E/E)	$\frac{2.05\%}{E(GeV)^{0.36}}$

Table 4.1: Properties of the Crystal Ball.

4.3 Particle Identification Detector (PID)

The PID shown in Fig. 4.7 is a cylindrical detector with **10 cm** inner diameter around the beam axis centered on the target within the *Crystal Ball*. It is comprised of **24** *plastic scintillators* each with the size **31 cm × 1.3 cm × 0.2 cm**. Optical isolation between each *scintillator* is achieved by wrapping each individually in a foil. Each of these scintillators is connected to a *Hamamatsu* **R1635** *photomultiplier* tube of thickness **10 mm**.

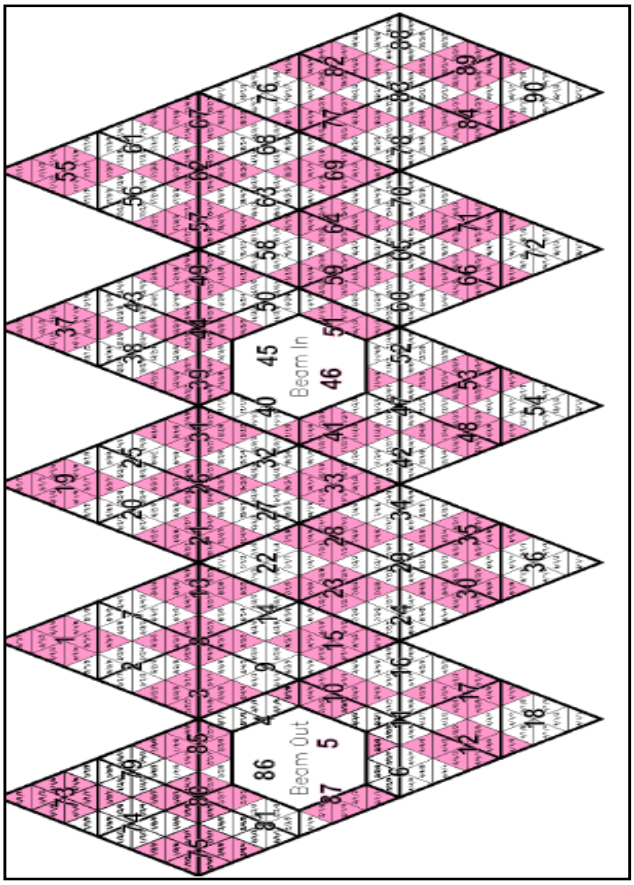

Figure 4.6: The two-dimensional Mercator-like projection of CB Crystals. It shows 90 shaded and unshaded groups of rectangles each containing eight crystals. It also shows the geometry of CB as there are 20 major triangles each of which is made of four minor triangles and each minor triangle contains nine crystals. The 'beam in' and 'beam out' hole is also visible.

The *PID* is installed inside the *Crystal Ball* for the purpose of identifying charged particles. This detector measures small energy losses (ΔE) in the thin plastic scintillators and a rough variation of the *azimuthal angle (φ)* of the charged particles. By considering this ΔE and the total energy deposited in the *Crystal Ball*, one can identify different charged particles. In our experiment we did not use the output of *PID* because our analysis involved only neutral particles.

Figure 4.7: The PID before inserting it into position within the CB

.

4.4 The TAPS detector

TAPS is a front-end detector for the *Crystal Ball* as it detects photons or any charged particles that escape from the exit hole of the ball. *TAPS* was designed and installed with the purpose to study high-energy photon beams as well as neutral mesons [28].

TAPS consists of several hundred hexagonally shaped BaF_2 detectors (see Fig. 4.8) each of length **25 cm** (equivalent to **12** radiation lengths) that can be arranged in different configurations. The combined photon detection set-up for the *Crystal Ball* and *TAPS* shown in Fig. 4.9 covers approximately **96%** of a complete sphere. Since many particles are emitted in the forward direction, this forward wall is useful to increase the overall detection efficiency.

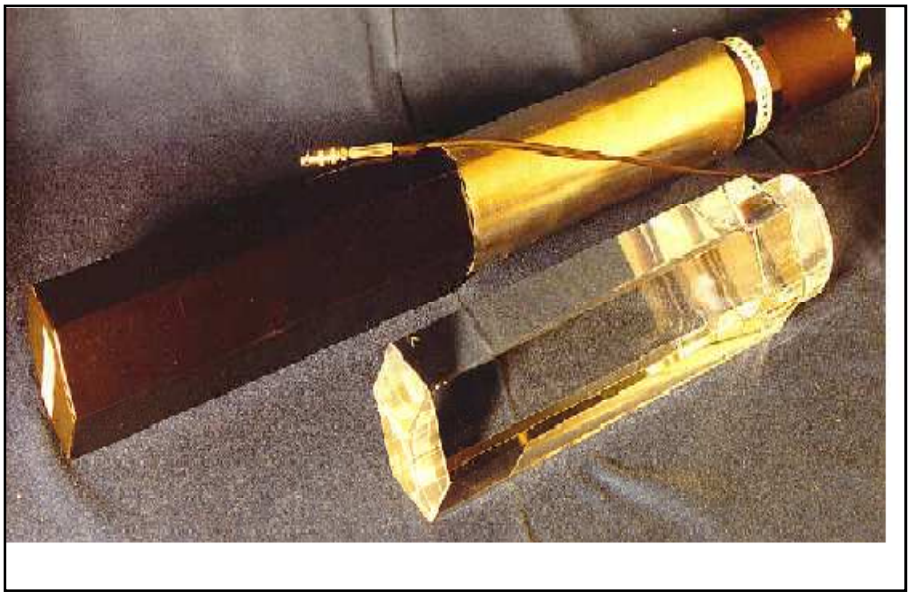

Figure 4.8: Each individual TAPS BaF_2 detector consists of a hexagonally shaped crystal tube of 25 cm in length with a 2.5 cm cylindrical end connected directly to the photomultiplier tube.

Because of some special characteristics of *BaF_2 crystals*, they are considered a good choice for the construction of *scintillation detectors*. First, *BaF_2* has a fast rise time of the scintillation pulse; because of this virtue the intrinsic time resolution (about 200 ps) of a single crystal is very good. The accurate particle identification using the time of flight of a particle is made using this essential feature of the *BaF_2 crystal*. Second, it produces scintillation light with two components: a fast component and a slow component, corresponding to decay times of **0.60 ns** (λ = 195 nm and 220 nm) and **620 ns** (λ = 310 nm), respectively. These characteristics of BaF_2 crystals provide a means to separate slower hadrons like protons and neutrons from the faster particles like photons, electrons, and pions by finding their corresponding time of flights. Particle identification using this technique of decay of short and long light components is generally called *pulse shape analysis (PSA)*. By integrating the light signals over a short and a long time gate, the pulse shape analysis is carried out.

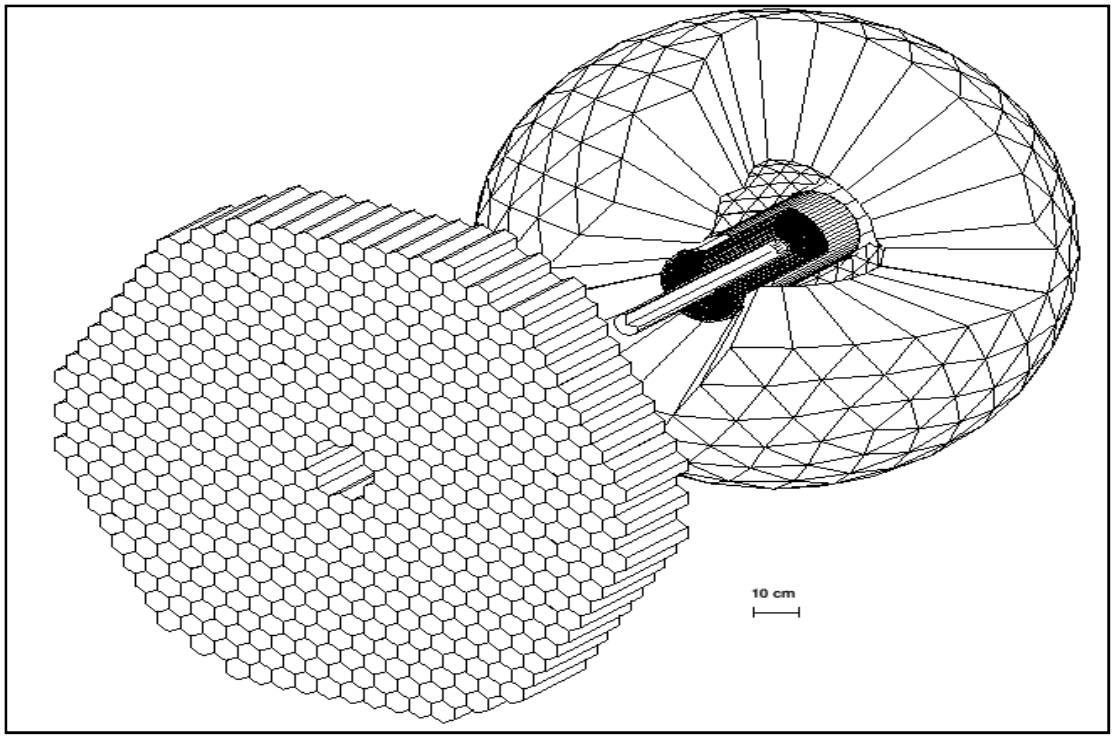

Figure 4.9: The use of TAPS as a forward wall detector at a distance 1.8 m from the CB. The 384 BaF_2 crystals of the TAPS forward wall cover the hole of the CB to cover ~ 96% of 4π in solid angle.

Because the relative intensity of the short component is higher for photons than for nucleons, the ratio of these two components provides a good tool to identify these particles as shown in Fig. 4.10. Third, BaF_2 has a high photon detecting efficiency and energy resolution over a wide range of energies. In addition, because of the high granularity of *TAPS*, there is a good position resolution.

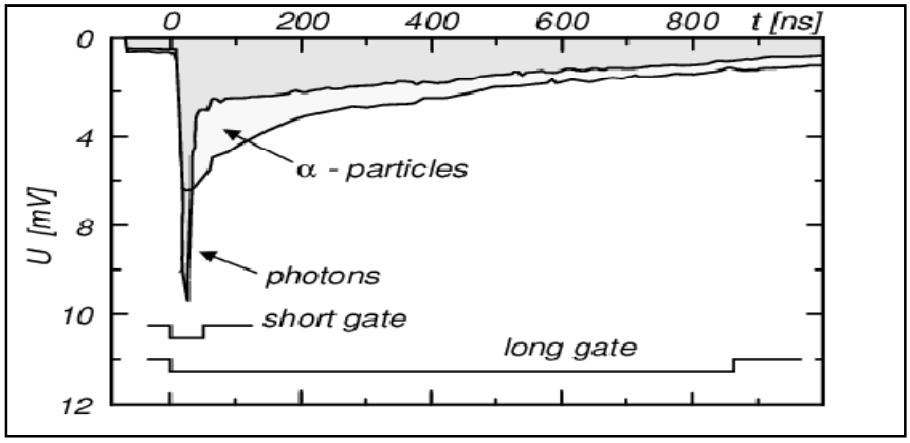

Figure 4.10: A schematic plot of the pulse shape for an α-particle and a photon in TAPS. The larger long component makes it possible to distinguish the α-particle and a photon.

Each of the *BaF_2 detectors* has hexagonal front and back shapes with a cylindrical end part of inner diameter **5.9 cm** as shown in Fig. 4.8. The surfaces of the crystals are polished. A UV reflector that is made up of eight layers of *PTFE3* and one layer of thin aluminum foil is wrapped around these crystals. The individual crystals are coupled to a *Hamamatsu R2059 photomultiplier* tube using silicone grease. In order to provide effective magnetic shielding up to a flux of **0.02T**, the phototubes and the cylindrical section of the crystals are completely surrounded by a magnetic shield. In front of each *BaF_2 detector*, a hexagonally shaped *5 mm* thick *NE102A plastic scintillator* is installed so as to distinguish between charged and neutral particles. These are called veto detectors. Some of the important properties of the TAPS detector are summarized in Table 4.2.

Distance from the center of CB	1.80 m
Polar angular acceptance	$2^\circ \leq \theta \leq 20^\circ$
Time resolution	0.5 ns FWHM
Angular resolution ($\sigma\varphi$)	0.7° FWHM
Energy Resolution ($\sigma E/E$)	$\frac{3.7\%}{E(GeV)^{\frac{1}{4}}}$

Table 4.2: Properties of TAPS

CHAPTER FIVE

Data analysis

This chapter explains the analysis software and Monte Carlo simulation used for our present work. For our dissertation, first we setup root environment in Red Hat Linux 5. All files were run in terminal. For photoproduction reaction $\gamma p \rightarrow \eta p \rightarrow \gamma\gamma p$ we choose suitable *dat* file, and made several *dat* files for different energy of striking gamma. Now these files were moved into *.hbook*. Again, these files made under *.hbook* were run to give *mkin* files. These *mkin* files were run under *cbsim*. These *cbsim* files were again run in *acqu*. From the histograms obtained from *acqu,* we studied photoproduction reaction $\gamma p \rightarrow \eta p \rightarrow \gamma\gamma p$.

5.1 Analysis software

5.1.1 ROOT

The root system provides a set of frameworks with all the functionality needed to handle and analyze large amounts of data in a very efficient way. Having the data defined as a set of objects, specialized storage methods are used to get direct access to the separate attributes of the selected objects. This allows the easy setup of an analysis system without having in touch the bulk of the data that can query and process the data interactively.

ROOT also provides a good environment to learn *C++*. *ROOT* helps to built acquisition, simulation and data analysis systems.

5.1.2 Importance of ROOT

The *ROOT* project was started as an analysis tools for the experiment of *CERN*. With *ROOT,* we can try to provide a basic framework that offers a common set of features and tools for all domains of high energy physics computing. Currently the emphasis of *ROOT* is on the data analysis. The system can easily be extended to

other domains like simulation, reconstruction and event displays. *ROOT* is an ideal environment to introduce physicists quickly to the new world of objects and *C++*.

5.2 AcquRoot

AcquRoot is the analysis software that is used for all of the online and offline analysis of data for *Crystal Ball* experiments at *MAMI*. It is an upgraded form of *ACQU* incorporating with the multi-threaded purely *C++* program mainly written by **J. R. M. Annand** [29]. *AcquMC* is a **Monte Carlo reaction** kinematics generator and *AcquDAQ* reads data from some components of the detector system and feeds the data to one or more central event builders. AcquRoot is based on the framework of *ROOT* [30], which is the *CERN C++* based suite of software and libraries. *ROOT* is based on object-oriented sources, comprised of various types of classes, each performing a specific task. As *AcquRoot* combines the full *ROOT* functionality, it makes extensive use of the facilities offered by *ROOT* for controlling *A2 electronics*, data acquisition, storage, retrieval, and analysis. The tree structure of the *AcquRoot* analyzer is shown in Fig. 5.1.

The four circles of different colors on the left-hand side of the figure represent the four important classes involved in *AcquRoot*. The lowest green circle represents a dedicated class specific to each detector: e.g., *Crystal Ball NaI* crystals detectors are accounted by the class *TA2CB NaI, TAPS* BaF_2 *crystals* by *TA2TAPS* BaF_2, focal plane tagger detectors by *TA2TaggLadder* and so on. These detector classes are responsible for conversion of the digitally stored pulse heights to energies and times. The blue circle, one step higher, represents the three classes that collect information from each of the three subgroups of the detectors. *TA2CrystalBall* represents the group of detectors related to the *Crystal Ball*. Similarly, *TA2TAPS* and *TA2Tagger* represent all the detectors related to the *TAPS* (e.g., BaF_2, *Veto*), and *the Tagger* (e.g., *Ladder, Pb Glass, Micro*), respectively.

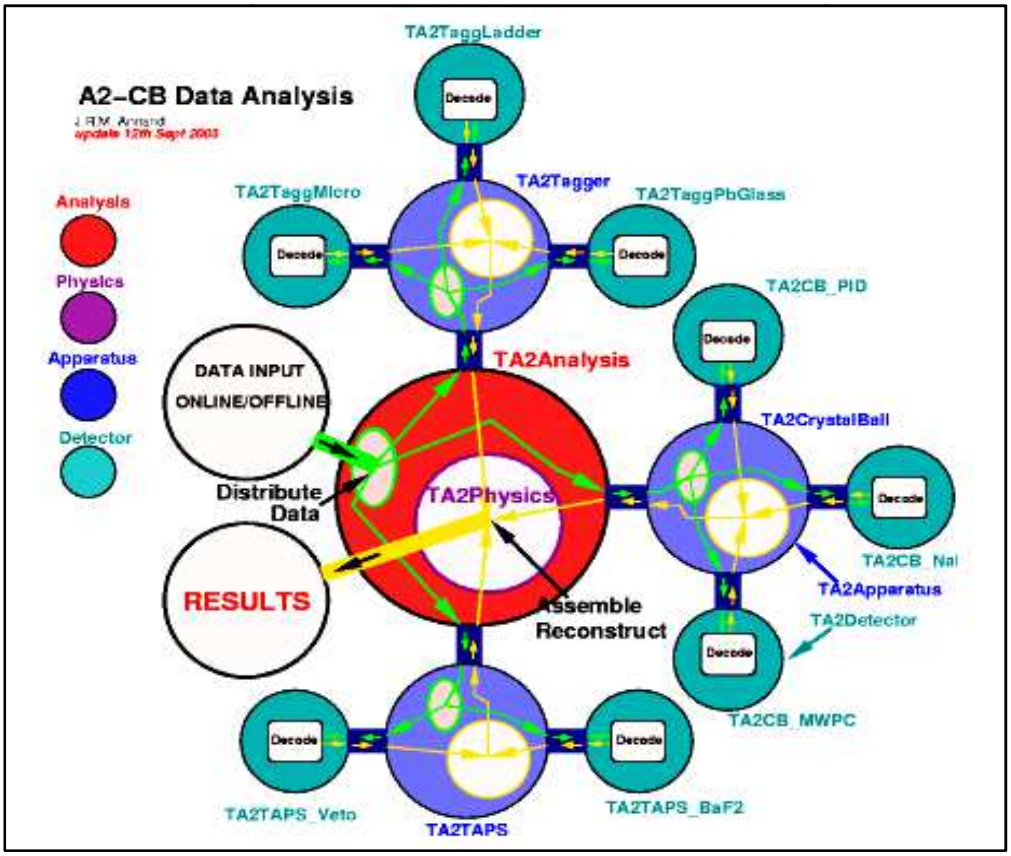

Figure 5.1: The tree structure of AcquRoot Analyzer with its Apparatus, Detector, Physics and Analysis classes [29].

These three classes in a group form a class called *TA2Apparatus, which* is responsible for the conversion of energies and times into particle types and four-vectors. The pink circle above the blue circle represents a Physics class that collects all the information from the three detector systems (such as four-vectors and particle identities) to reconstruct the related events yielding the invariant and missing mass to identify the specific particle. The red circle on the top represents a class called *TA2Analysis* which provides the core of the data analysis system. It decodes the basic *ADC, TDC,* and *Scalars information* and passes them to *TA2Apparatus*.

5.3 Monte Carlo simulation

Monte Carlo methods (or **Monte Carlo experiments**) are a class of computational algorithms that rely on repeated random sampling to compute their results. Monte Carlo methods are often used in computer simulations of physical and mathematical systems. These methods are most suited to calculate by using a computer and tend to be used when it is infeasible to compute an exact result with a deterministic algorithm. This method is also used to determine theoretical derivations.

Monte Carlo methods are especially useful for simulating systems with many coupled degrees of freedom, such as fluids, disordered materials, strongly coupled solids, and cellular structures. They are used to model phenomena with significant uncertainty in inputs, such as the calculation of risk in business. They are widely used in mathematics, for example to evaluate multidimensional definite integrals with complicated boundary conditions. When **Monte Carlo simulations** have been applied in space exploration and oil exploration, their predictions of failures, cost overruns and schedule overruns are routinely better than human intuition or alternative "soft" methods [31].

There were two parts to the **Monte Carlo simulations**, the *event generation* and the *particle tracking*.

As the first step, a program was used to generate the kinematics of events. The input parameters were the target dimensions, mass, and density, also the beam energy, spot size at the target, as well as the beam divergence, for this we used real “beam triggers “recorded in the course of the experiment.

The second step used a program based on the *CERN package GEANT*, *version3.21*, that reads the output of the first program and tracks all particles through volumes of different materials, in a setup that mimics as closely as possible the actual experimental setup. The geometries included were the *CB; TAPS, TAPS veto wall, PID* and *the target* (see chapter 4) [32].

CHAPTER SIX

Results and Discussions

This chapter presents the study of photoreaction $\gamma p \rightarrow \eta p \rightarrow \gamma\gamma p$. In this events for $\gamma p \rightarrow \eta p$ were simulated using the **Monte Carlo analysis**. Since the threshold, photon energy for $\gamma p \rightarrow \eta p$ is **702.77 MeV (**see chapter 3.4), we have to provide energy of incident photon beam just greater than threshold energy for η meson production. The ηp final state is obtained through the following sequential decays:

$$\gamma p \rightarrow \eta p \tag{6.1}$$

and η further decays into two γ as

$$\eta \rightarrow \gamma\gamma \tag{6.2}$$

so our final decay becomes

$$\gamma p \rightarrow \underset{①}{\eta} \quad p \rightarrow \underset{③}{\gamma} \quad \underset{④}{\gamma} \quad p \tag{6.3}$$

where ① ⇒ eta produced as first particle

②⇒ Proton produced as second particle

③⇒ Gamma produced as third particle

④⇒ Gamma produced as fourth particle

With reference to the threshold energy, we create an environment to provide energy of photon more than threshold i.e. more than **702.77 MeV**. In our study we started from **735 MeV** and within the interval of **35** i.e. **770, 805, 840, 875, 910, 945, 980, 1015, 1050, 1085, 1120, 1155, 1190, 1225, 1260, 1295, 1330, 1365** and **1400 MeV** data were taken. In our reaction $\gamma p \rightarrow \eta p \rightarrow \gamma\gamma p$ particle are kept according to ***GEANT*** *id* such that

$\gamma = 1$

$p = 14$

$\eta = 17$

The **GEANT ids** of different elementary particles are given in Table 1. 4.

For the reaction $\gamma p \rightarrow \eta p \rightarrow \gamma\gamma p$ we have to provide suitable value of photon energy **≥ 702.77 MeV**. That beam of photon is incident on *liquid hydrogen target* and produces two *photons* and *proton*. Since we are doing this process through simulation, we provide such environment through *dat* file. One of the examples of *dat* file is shown in Appendix **[A.1]**.

We made several *dat* files. Now these made files were run under *./deck_kin* in *mami_mcarlo/deckin*. The high-energy photon incident on *liquid hydrogen target* 50000 times. The events were generated for each energy value from **735 MeV** to **1400 MeV.** After that, we move these files to *results_deckin*. Where we used command e.g

mv ._hbook ../results_deckin/deckin_newetagama_735.hbook

mv _.hbook ../results_deckin/deckin_newkris_770.hbook etc

These files made under *hbook* are converted into root files using command *h2root deckin_newetagama_*e.g. hbook *newkris.e.g.root*., where e.g. can take any value from energy range **735** to **1400 MeV** that were included in *dat* files. These give different histograms which are shown below.

6.1 Event generation by using mkin software

After converting *hbook* files into *root* files we study whether the basic needs for our reaction is fulfilled or not. By studying the nature of histograms obtained from *root* files, we can conclude that events are generated according to our photoreaction $\gamma p \rightarrow \eta p \rightarrow \gamma\gamma p$. Actually all *root* files corresponding to different *dat* files for each energy values generate events. Among them, one *root* file corresponding to energy value **1400 MeV** is taken as example. In this *root* file, we can see different histograms, which are depicted below.

6.1.1 Generation of η meson as particle ①

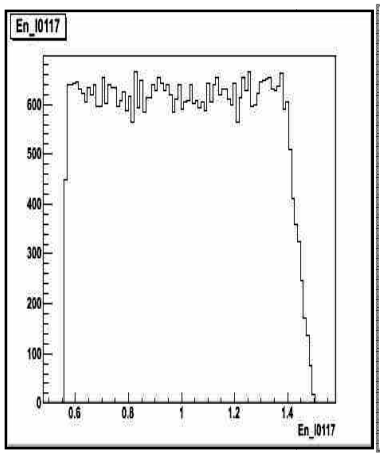

Figure 6.1: Energy of eta meson produced as particle ①

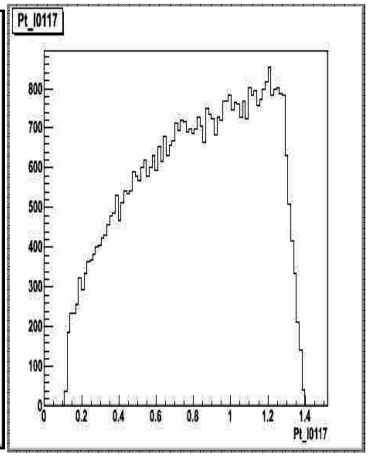

Figure 6.2: Transfer momentum of eta produced as particle ①

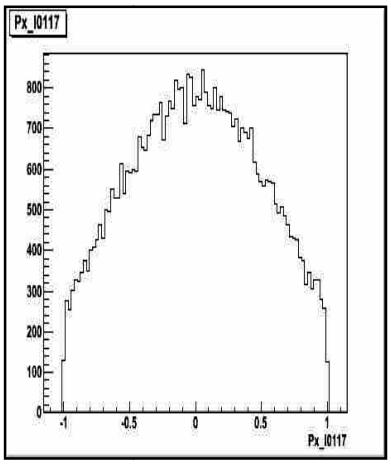

Figure 6.3: Momentum of eta along x-direction as particle ①

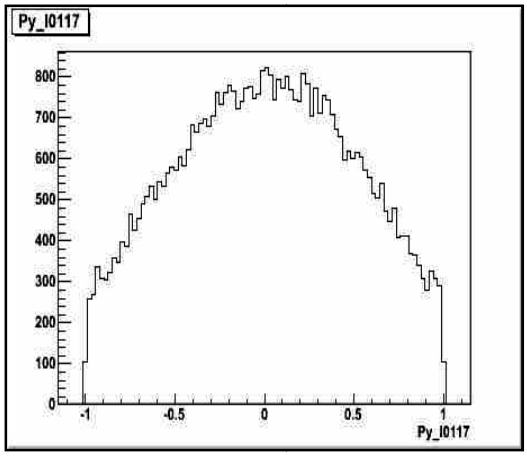

Figure 6.4: Momentum of eta along y-direction as particle ①

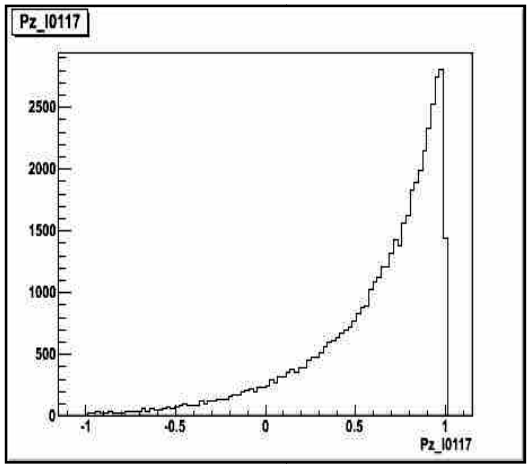

Figure 6.5: Momentum of eta along z-direction as particle ①

Referring to Eq. (6.3), we have provided an environment to the photoreaction $\gamma p \rightarrow \eta p \rightarrow \gamma\gamma p$ in *dat* file. According to this reaction, η was first produced particle. Figures 6.1 to 6.5 show that *eta meson* produced as first particle. In each figures we can see a code as **10117**. In these five figures code **17** (last two digit in code) represent *eta meson* produced. Middle 1 in code **10117** denotes first produced particle. E_n represents energy, P_t represents transfer momentum, P_x, P_y and P_z represents momentum along x-, y- and z-direction respectively in our photoreaction $\gamma p \rightarrow \eta p \rightarrow \gamma\gamma p$.

6.1.2 Generation of proton as particle ②

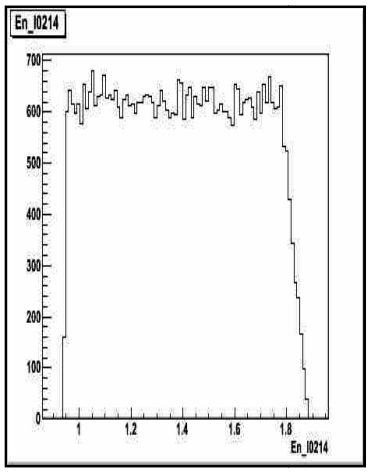

Figure 6.6: Energy of proton as particle ②

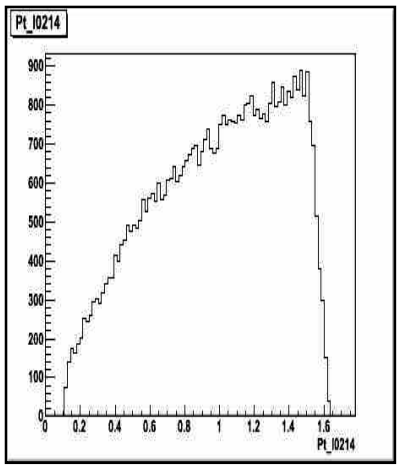

Figure 6.7: Transfer momentum of proton produced as particle ②

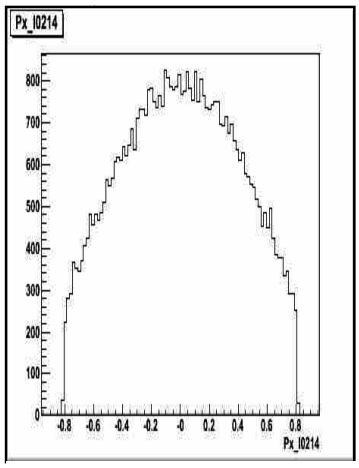

Figure 6.8: Momentum of proton along x-direction as particle ②

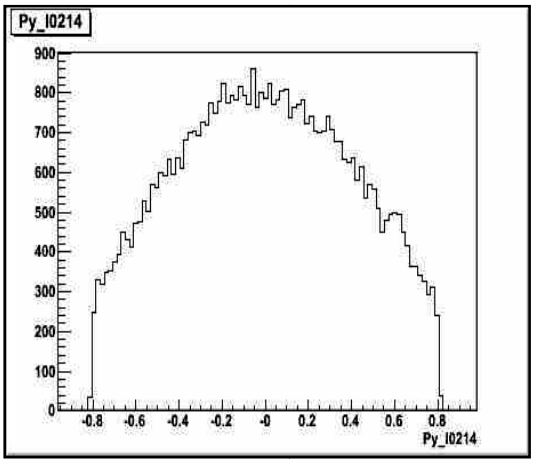

Figure 6.9: Momentum of proton along y-direction as particle ②

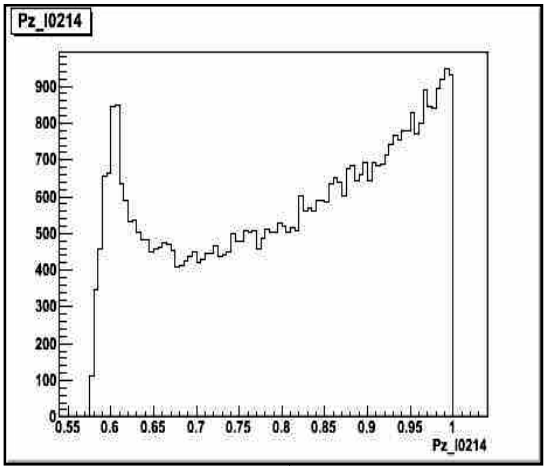

Figure 6.10: Momentum of proton along z-direction as particle ②

Considering the Eq. (6.3), proton was the second produced particle in the reaction $\gamma p \rightarrow \eta p \rightarrow \gamma\gamma p$. In the histograms obtained from *root* file proton can be seen as second produced particle. In above figures code-**10214**, **14** refer to **GEANT** id of proton and middle **2** in **10214** represents second produced particle. E_n represents energy, P_t represents transfer momentum, P_x, P_y and P_z represents momentum along x-, y- and z-direction respectively in our photoreaction $\gamma p \rightarrow \eta p \rightarrow \gamma\gamma p$.

6.1.3 Generation of gamma as particle ③

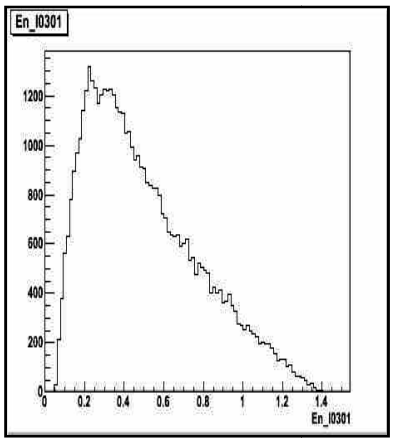

Figure 6.11: Energy of photon produced as particle ③

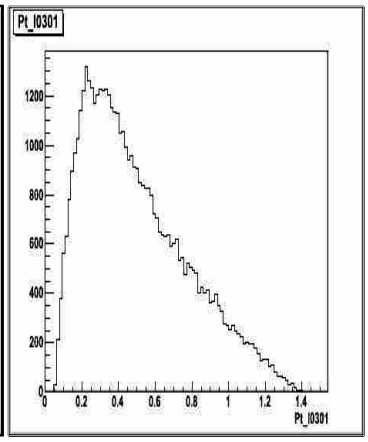

Figure 6.12: Transfer momentum of photon produced as particle ③

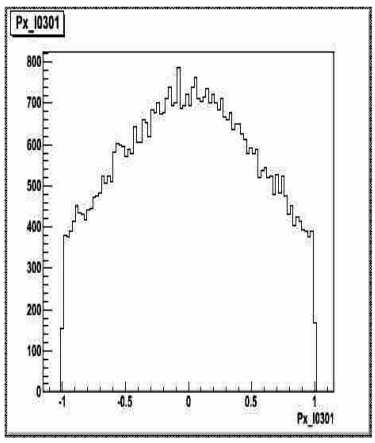

Figure 6.13:Momentm of photon along x-direction as particle ③

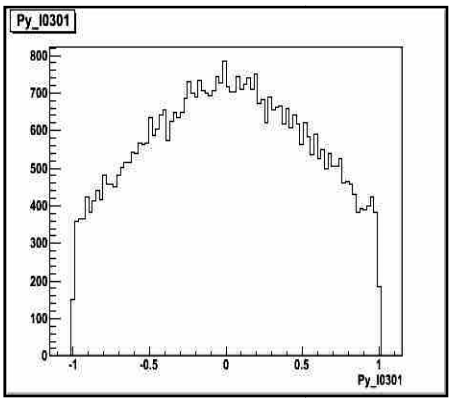

Figure 6.14: Momentum of photon along y-direction as particle ③

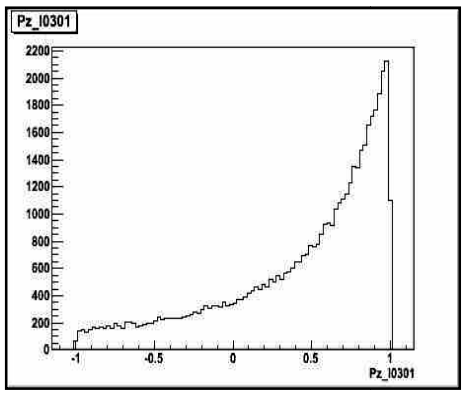

Figure 6.15: Momentum of photon along z-direction as particle ③

Referring to Eq. (6.3), we have provided an environment to the photoreaction $\gamma p \rightarrow \eta p \rightarrow \gamma\gamma p$ in *dat* file. According to this reaction, photon was third produced particle. Figures 6.11 to 6.15 show that photon was produced as third. The **GEANT** id of photon is 1. In these five figures code **10301** (last two digit **01**in code) represent photon was produced. Digit 3 in each code **10301** denotes third produced particle. E_n represents energy, P_t represents transfer momentum, P_x, P_y and P_z represents momentum along x-, y- and z-direction respectively in our photoreaction $\gamma p \rightarrow \eta p \rightarrow \gamma\gamma p$. The nature of energy histogram and transfer momentum histogram are exactly similar. This indicates that energy is transferred into momentum.

6.1.4 Generation of gamma as particle ④

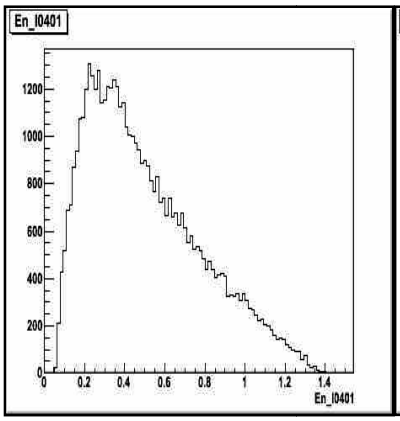

Figure 6.16: Energy of photon produced s particle ④

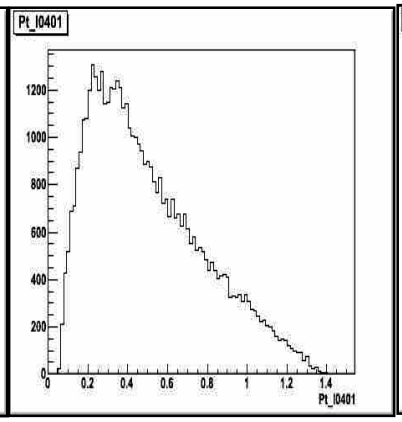

Figure 6.17: Transfer momentum of photon produced as particle ④

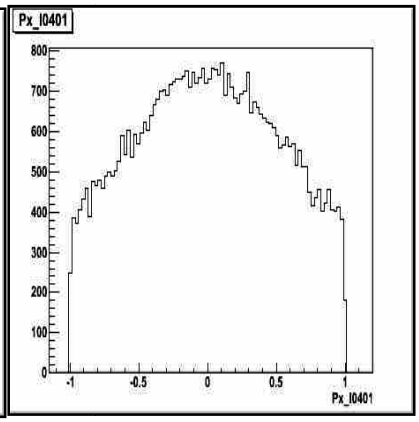

Figure 6.18: Momentum photon along x-direction as particle ④

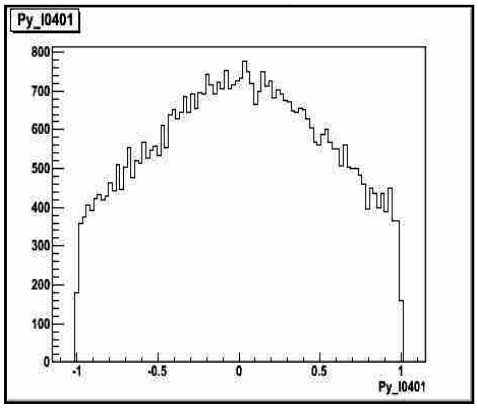

Figure 6.19: Momentum photon along y-direction as particle ④

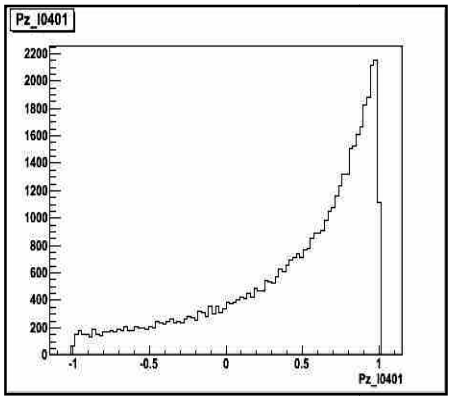

Figure 6.20: Momentum photon along z-direction as particle ④

Above figures from 6.16 to 6.20 show that photon was produced as fourth particle. In each figures the code **10401** is present. The last two digits 01 in 10401 represent **GEANT** id of photon and **4** in **10401** represents photon was produced as fourth particle. E_n represents energy, P_t represents transfer momentum, P_x, P_y and P_z represents momentum along x, y and z direction respectively.

From the figures from 6.1 to 6.20 show that 4 particles were generated namely eta meson as ①, proton as ②, photon as ③ and another photon as ④.In these figures the nature of energy histogram and transfer momentum histogram are similar which indicates that the energy is transferred to the momentum.

6.1.5 Generation of photon beam

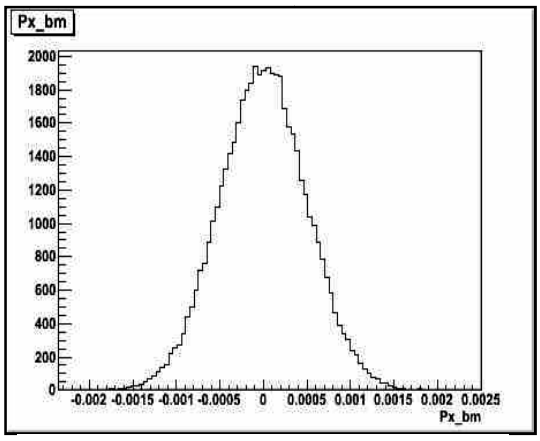

Figure 6.21: Momentum of beam along x-direction

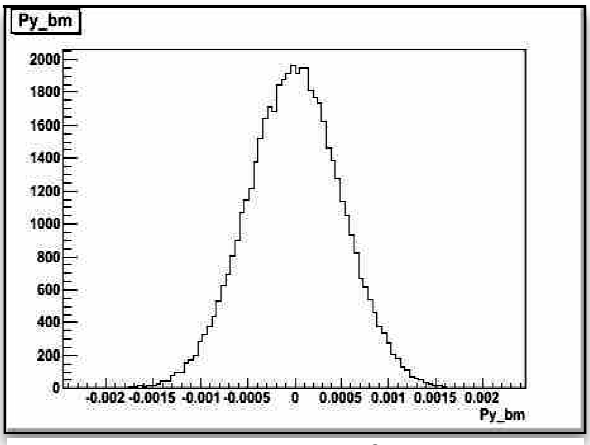

Figure 6.22: Momentum of beam along y-direction

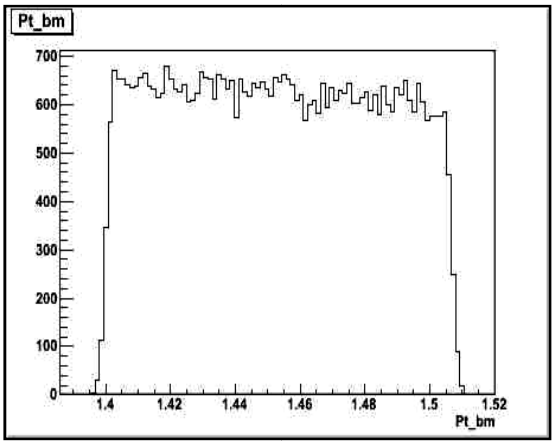

Figure 6.23: Transfer momentum of beam

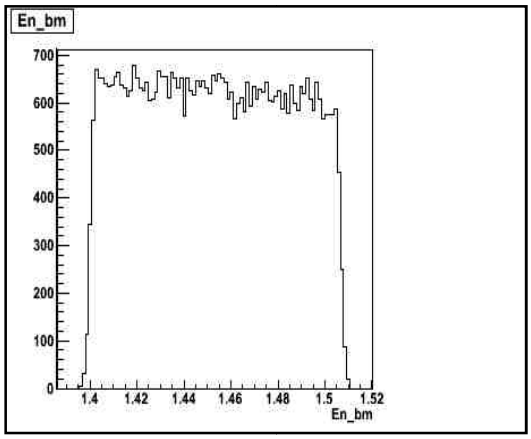

Figure 6.24: Energy variation of beam

Above figures from 6.21 to 6.24, show the nature of incident beam of photon. Fig.6.21 and Fig. 6.22 show the momentum of beam along x- and y-direction respectively. Fig. 6.23 and Fig. 6.24 show the transfer momentum of beam and energy of beam. The nature of energy variation of beam and transfer momentum of beam is quite similar. This indicates that the energy of beam is transferred to the momentum in the photoreaction Eq. (6.3).

6.1.6 Generation of target vertex

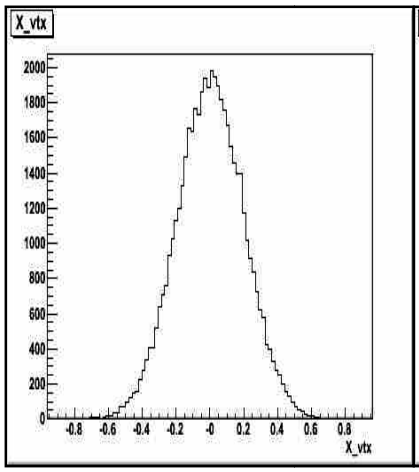

Figure 6.25: X- vertex

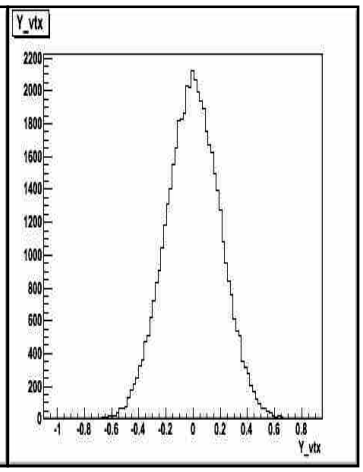

Figure 6.26: Y- vertex

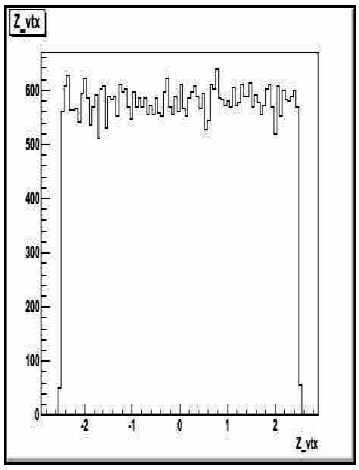

Figure 6.27: Z- vertex

Above figures from 6.25 to 6.27 show the vertices made along x-direction, y-direction and z-direction when beam of photon incident on the target in the photo reaction $\gamma p \rightarrow \eta p \rightarrow \gamma\gamma p$ The nature of vertex made along x- and y- direction is found similar.

6.2 Event identification by using cbsim software

The files generated in *deckin* files are detected by using *cbsim* software. For this, we have to run these *mkin* files into *cbsim.* In *mkin* file, we made necessary correction. We choose *gamaeta.ffcards* files in *mkin*. One mkin file is as shown in Appendix **[B.1].**

In *mami_mcarlo/jb_ffcards files/gamaeta_ffcards* files Appendix **[C.1]** we choose suitable *TRUE/FALSE* option according to our reaction.

Then we run our files using command *./mkin_run_good.sasha*.e.g. Where e.g. represents energy values **735MeV**, **770MeV**, or **805 MeV** ...**1400MeV**. After running these files, we check the particles through their **GEANT** id (See Table 1.3). Results of *cbsim* file in form of histograms are shown in Fig. 6.28 to Fig.6.37 below.

6.2.1 Particle identification

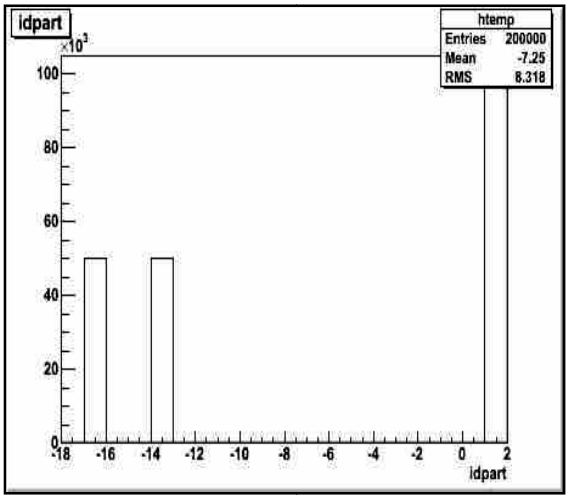

Figure 6.28: Identification of produced particle in γp → ηp → γγp

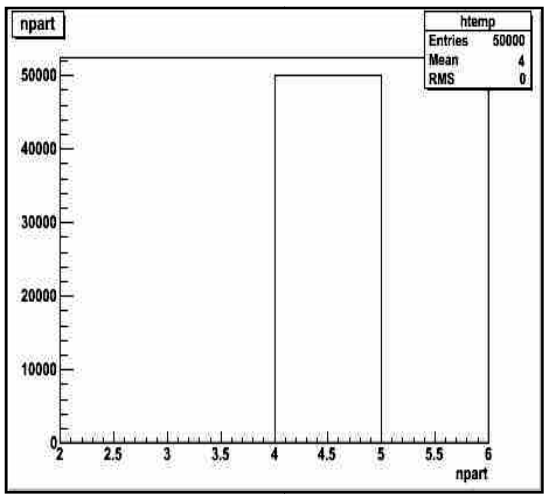

Figure 6.29: Number of particles produced in γp → ηp → γγp

Fig.6.28 shows that the identification of particles in the reaction γp → ηp → γγp. Histogram 6.28 shows there is height at points **1**, **14** and **16**. **1** means **GEANT** id of *photon*, **14** means **GEANT** id of *proton* and **17** means **GEANT** id of *eta meson*. This means we had used these three particles in *dat* file. These particles are detected in *cbsim*. Fig. 6.29 shows that number of particles involved in *eta* meson photoproduction. There is starting of height from point **4**, it means **4** particles were involved in the reaction γp → ηp → γγp. These two facts detected as true because the same number of particles i.e. **4** and same particles i.e. *eta meson*, *proton* and *photon* are producing that also were used in *dat* file.

6.2.2 Vertex identification

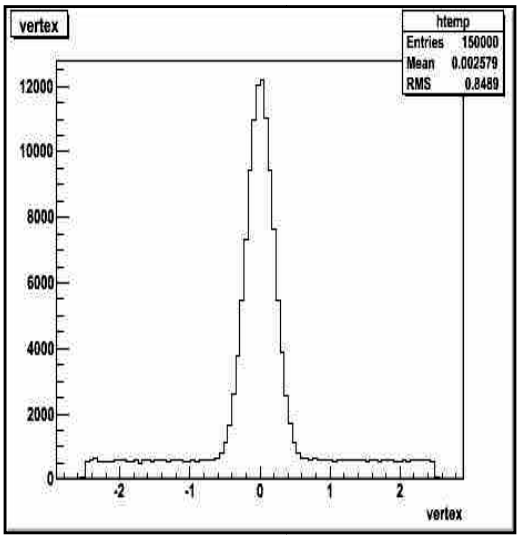

Figure 6.30: Vertex made by hitting the target by incident photon

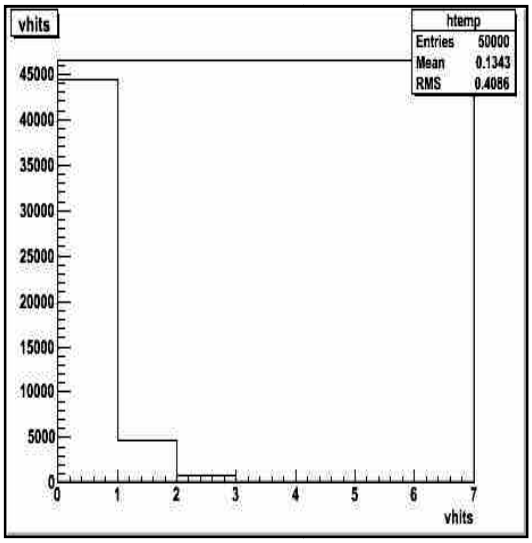

Figure 6.31: Maximum hit by gamma to the target

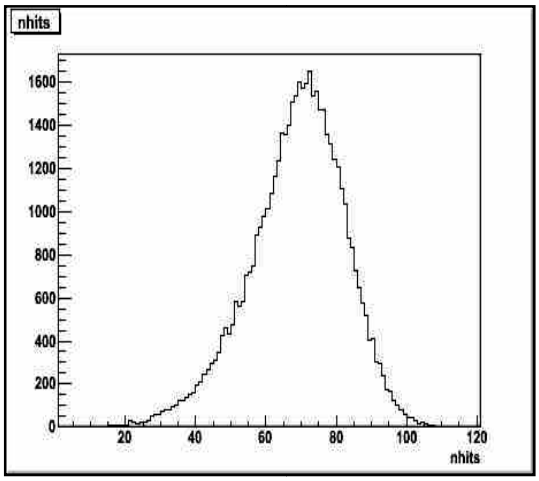

Figure 6.32: Number of times hit by beam of photon to the target in the photoreaction $\gamma p \rightarrow \eta p \rightarrow \gamma\gamma p$

Fig. 6.30 shows the vertex made by hitting the target by photon beam. The peak is at origin implies that the incident beam mostly incident at the centre of the target.Fig. 6.31 shows that maximum hit by photon beam to the target. The height is maximum at origin implies that photon beam is incident at the centre of the target. Fig. 6.32 shows the average number of hits by the incident beam to the target. It shows the average number of hit is approximately 60.

6.2.3 Detection of energy and momentum

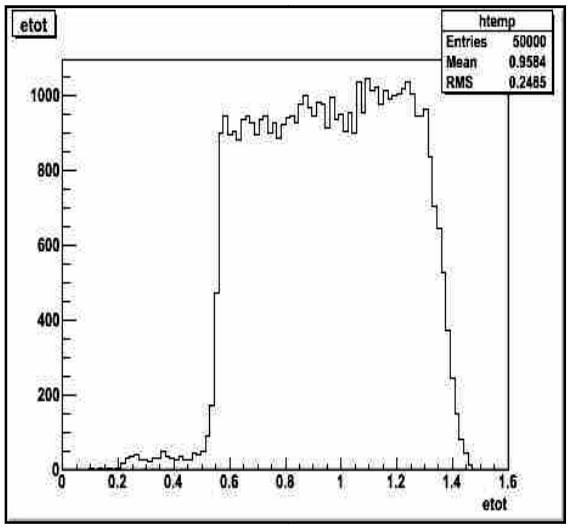

Figure 6.33: Total energy variation

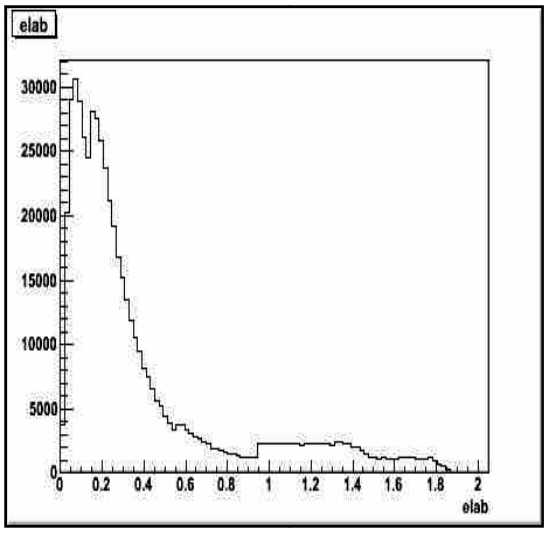

Figure 6.34: Distribution of energy in lab

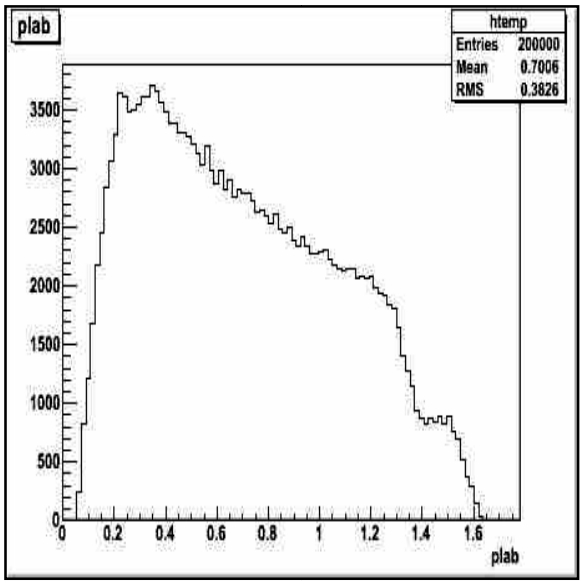

Figure 6.35: Distribution of momentum in lab

Fig. 6.33 shows the variation of total energy . This figure is similar to the Fig. 6.24 (energy of the beam). The same type of beam what is generated at *mkin* is detected at *cbsim* Fig. 6.34 shows that distribution of energy in lab and Fig. 6.35 shows distribution of momentum in lab.

6.2.4 Crystal Ball and TAPS detector as prime detectors

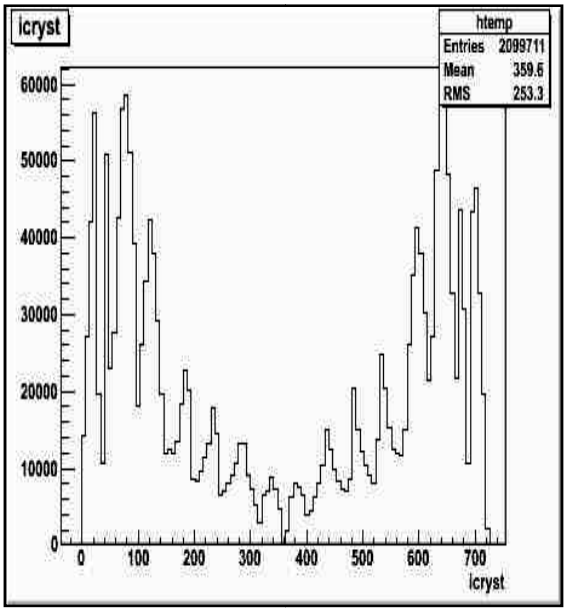

Figure 6.36: Position of elements of NaI crystal in Crystal Ball

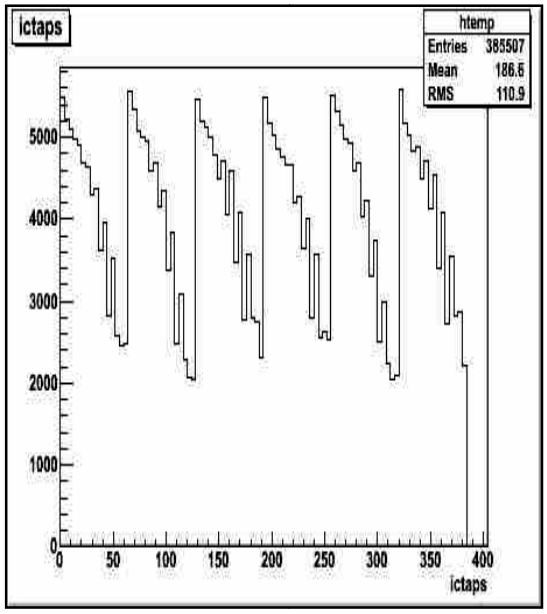

Figure 6.37: Position of elements of BaF_2 crystal in TAPS

Fig. 6.36 shows that the position of **720** elements of NaI crystal in *Crystal Ball*. Fig. 6.37 shows distribution of position of **384** elements of **BaF_2** crystal in **TAPS.**

From these figures from 6.28 to 6.37 we see that the files generated in *deckin* are detected in *cbsim*.

In above figures:-

etot⇒ total energy, id part ⇒ GEANT ids of particles involved in reaction

dircos⇒ direction cosine

From id part figure we can see proton, eta and gamma are involved in our reaction.

Now we have to run these files in *acqu*. Before this, we have to make necessary correction in *acqu/root/src/TA2PhotoPhysics.cc* and *acqu/root/src/TA2PhotoPhysics.h*. Similarly energy range, mass range etc correction were made in *acqu/data/CBphysics.dat*. Similarly, we provide the correct path and name in *acqu/data/CBMC.Offline*. One *CBMC* file is shown [**D.1**] and then we run our files in *acqu* using command *Acquroot --offline CBMC.Offline*. These files made

in *acqu* are moved in *root* according to our name for easy detection of our files with their respective energy.

Now we see our result in *root*. In *root* we choose command *root* (our files name made in acqu) for different energy value of gamma. We check our result for one energy value. Similar steps were performed for all values of energy.

Next we have to merge these all files to get combined result in the energy range (**735 MeV** to **1400 MeV**) .We change in *acqu/data/rootmerge.C*. First we make four combined result from **735** to **875, 910 to 1050, 1085 to 1225 and 1260 to 1400 MeV** and then we finally combined these four files into one to get the combined result from the energy range **735** to **1400 MeV**.

6.3 Reconstruction of events using AcquRoot software

After detection of events in *cbsim* we run these files in *acqu*. *Acqu* collects all the information from the *TA2Crystal Ball* (group of detectors): (see 5.2). After detection *acqu* reconstruct the related events yielding the invariant and missing mass to identify the specific particle. These yielding events as results are given below.

6.3.1 Mass of two gamma curve

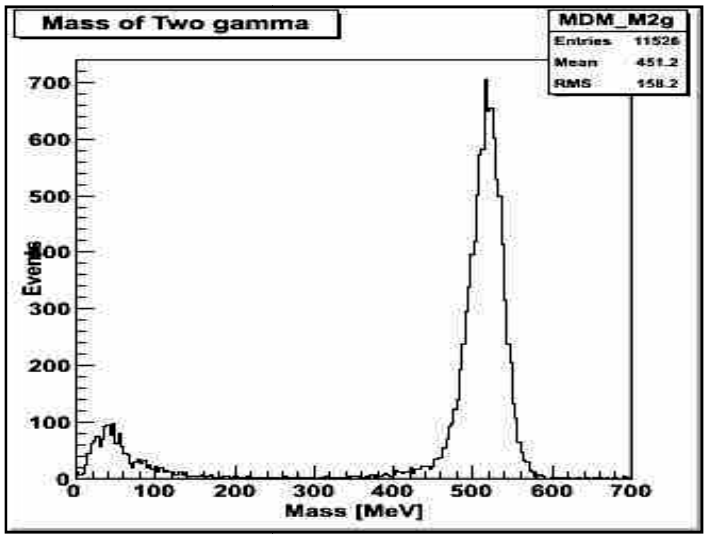

Figure 6.38: Mass of two gamma in the reaction γp → ηp → γγp

Mass of two gamma curve is drawn events versus Mass (in **MeV)**. This is the result of combination of all files made in *acqu* in the energy range from **735 MeV** to **1400 MeV**. There is peak in between **500** to **600 MeV**. It means the peak is approximately equal to mass of *eta meson* i.e.**550 MeV**. Since we know the mass of *eta meson* is **550.095 MeV/c^2**. In our study of photoreaction is γp → ηp → γγp, photon beam is incident on the liquid hydrogen target and produces *eta meson* and *proton*. The mid event ηp could not be detected by the detectors in the *Crystal Ball* and *TAPS* because the lifetime of *eta meson* is very short i.e.**10^{-18}s**. After decaying of *eta meson*, two *photons* were detected in *Crystal Ball and TAPS*. The detected mass of two gammas is near to the invariant mass of *eta meson* as shown in Fig. 6.39.

6.3.2 Mass of proton curve and thetaCM curve

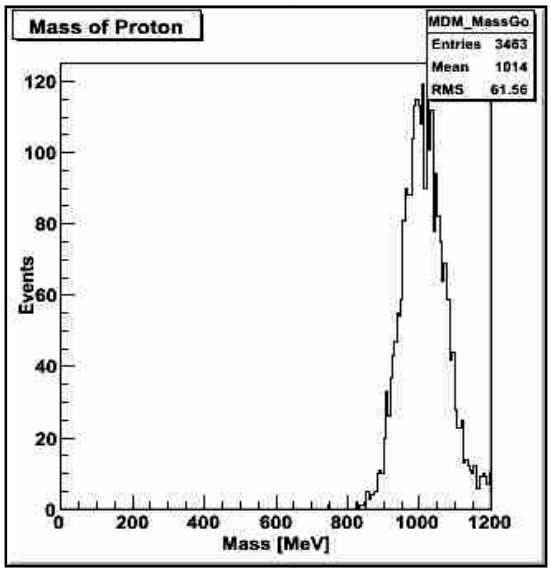

Figure 6.39: Mass of proton curve in the reaction $\gamma p \rightarrow \eta p \rightarrow \gamma\gamma p$

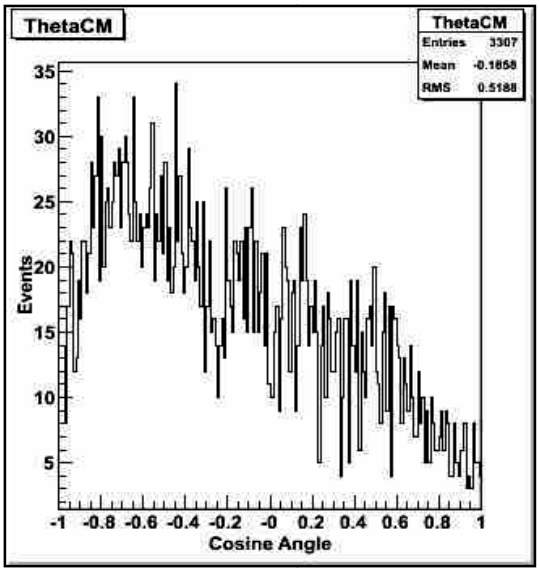

Figure 6.40: ThetaCM curve reaction $\gamma p \rightarrow \eta p \rightarrow \gamma\gamma p$

The *acqu* yields mass of proton curve, which is drawn events versus *Mass* (in MeV). This is another result of combinations of all files made in *acqu* in the energy range from **735 MeV** to **1400 MeV**. In Fig. 6.39, the peak of the curve is in between **900** to **1000 MeV**. Since mass of proton is **938.27 MeV/c^2**. The mass of curve from *acqu* is approximately equal to the mass of proton. It clarifies that proton was also produced in our studied reaction $\gamma p \rightarrow \eta p \rightarrow \gamma\gamma p$ and justifies the possibility of our reaction. In other words certainly our reaction has occurred. Fig. 6.40 is the thetaCM curve obtained from *acqu* is drawn events versus cosine angle. This cosine angle refers to the angle made by *eta meson* with the direction of incident photon beam.

6.3.3 Results obtained from TAPS and Crystal Ball

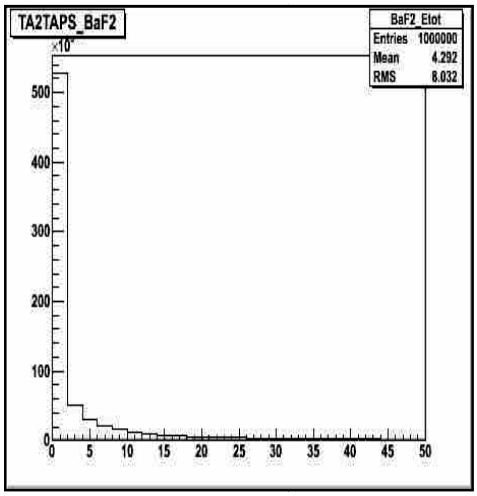

Figure 6.41: Variation of total energy of BaF_2 crystals in TAPS

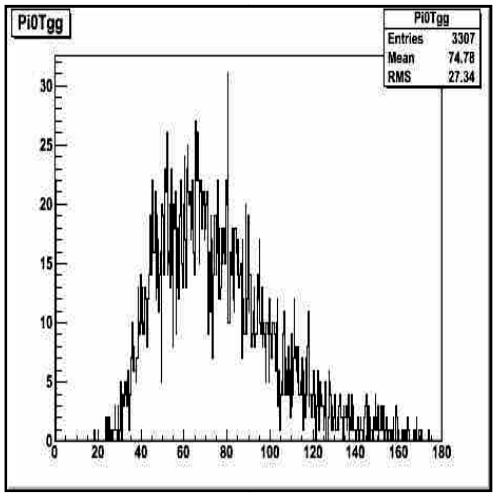

Figure 6.42: Variation of angle between two produced photon

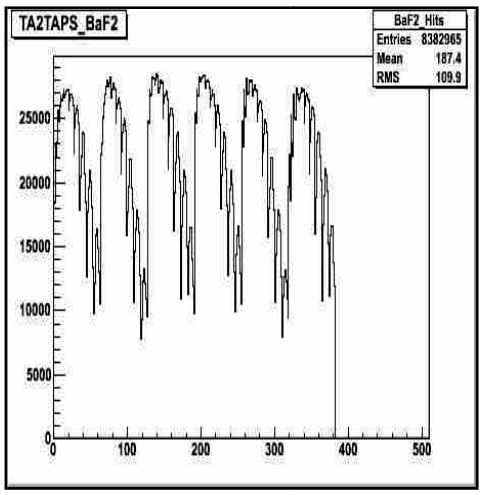

Figure 6.43: Position of elements of BaF_2 crystals in TAPS

Fig. 6.41 shows that energy measured by **384** elements of *BaF_2 Crystal*. Because of having the property of high energy resolution of **BaF_2** detects the particle with the help of corresponding energy value. The energy is near to **500 MeV**, it means mass of eta is near to **550 MeV**. It means eta meson was detected by *BaF_2* crystal. Fig. 6.42 shows variation of angle between two produced photon. It shows the peak is below 90˚ so we can say that there is low angle variation in produced photons. Figure 6.43 shows that position of **384** elements of *BaF_2 crystal in TAPS.* The result obtained from *cbsim* (Fig.6.37) software and *acqu* software (Fig. 6.43) matches almost.

6.3.4 Results related with NaI Crystal in Crystal Ball

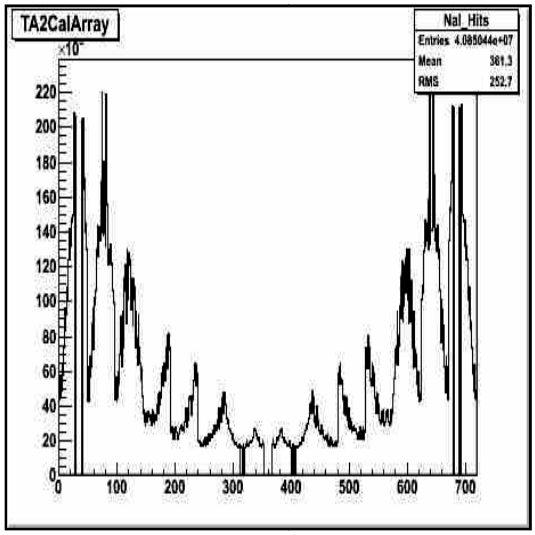

Figure 6.44: Position of elements of NaI crystal in Crystal Ball

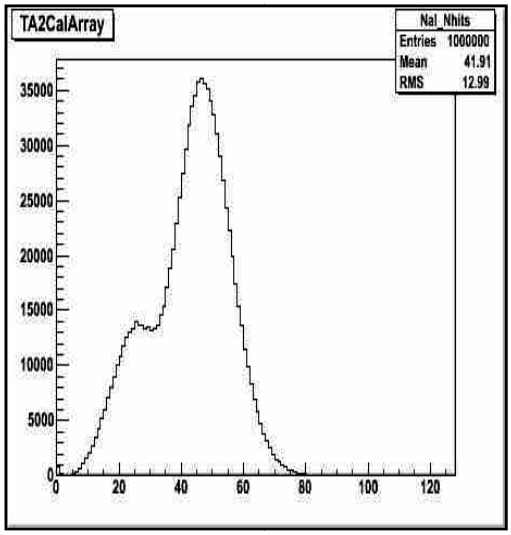

Figure 6.45: Average number of hits by the incident photon to the NaI crystal

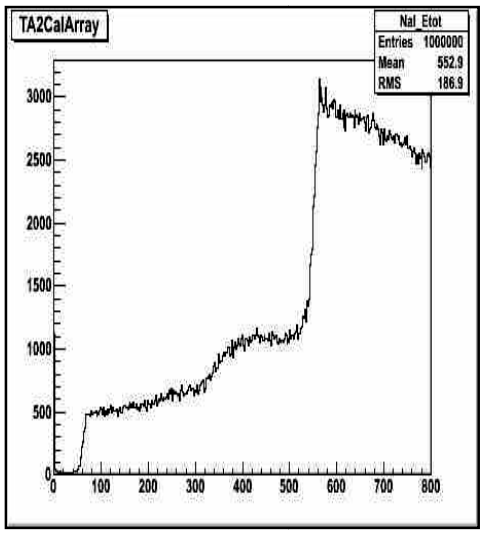

Figure 6.46: Total energy variation in the NaI crystal

Fig. 6.44 shows position of **720** elements of **NaI crystal**. Fig. 6.45 shows that average number of hits by the incident photon to the **NaI crystal**. In addition, the average hit is about 50. Fig. 6.46 shows that the energy deposited in the NaI crystal. After incident of photon beam to the target, some energy deposition occurs in the **NaI crystal**. There is higher deposition of energy at the end and lower in the middle.

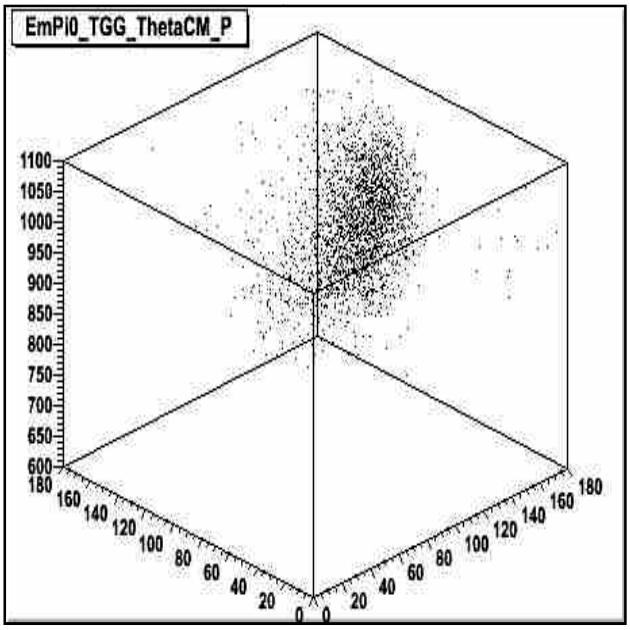

Figure 6.47: Three-dimensional figure of the missing mass of pi0 (or two gamma), angle between two photons and thetaCM

This three dimensional Fig. 6.47 shows that variation of ThetaCM, variation of angle between two photons and variation of missing mass of *eta meson*. Missing mass of *eta meson* (in figure missing mass of Pi0) gives mass of *proton*. Two axes in the plane shows the variation of angle thetaCM which is the angle made by *eta meson* with the target and angle between two photons and in vertical axis the dark part corresponds to the missing mass of *eta meson* or mass of proton in the photoreaction $\gamma p \rightarrow \eta p \rightarrow \gamma\gamma p$. The dark part corresponds to **950 MeV**, gives mass of proton in vertical axis. The dark part corresponds to the angle below 90˚in two horizontal axis shows that there is low angle variation in angle made between two protons as well as angle made by eta meson with incident photon beam.

6.4 Comparison of results with the previous measurements

6.4.1 Comparison of position of elements of NaI crystal

We compared our results of position of elements of NaI crystal detector in *Crystal Ball* (which is virtual detector) with the experimental result obtained at MAMI-C. The result of experiment is based on the real data taken in 2007 [13].

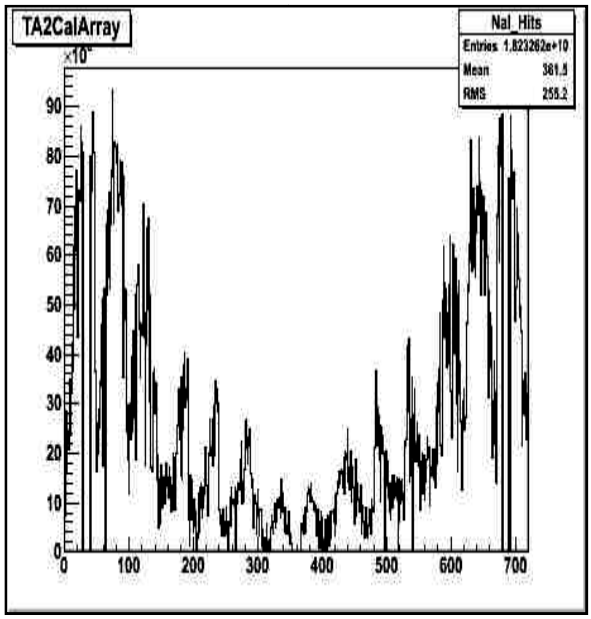

Figure 6.48: Experimental data of position of elements of NaI Crystal [13]

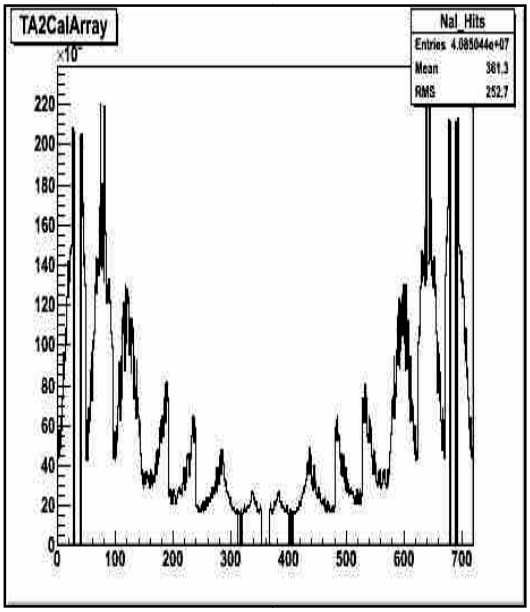

Figure 6.49: Our result of position of elements of NaI crystal obtained by Monte Carlo Simulation

By observing the histograms shown above in Fig. 6.48 and Fig. 6.49, we can found that there is an approximate similarity between experimental data and result obtained by using **Monte Carlo simulation**. Both figures explain to facilitate position of elements of **720** elements of *NaI crystal* in *Crystal Ball*. Both figures are quite similar. It is an interesting result, both experimental and our result matches. The events measured by NaI are helpful to measure the energy deposited due to the incident of high-energy photon to the NaI crystal.

6.4.2 Comparison of position of elements of BaF_2 crystal

We compared our results of position of 384 elements of BaF_2 crystal detected by virtual detectors using **Monte Carlo Simulation** with of experimental position of elements of BaF_2 crystal.

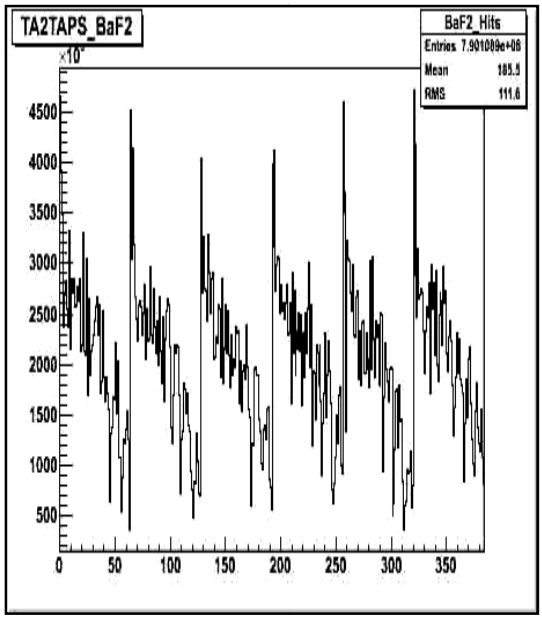

Figure 6.50: Position of elements of the 384elements of BaF_2 Crystals in the TAPS experimentally [13]

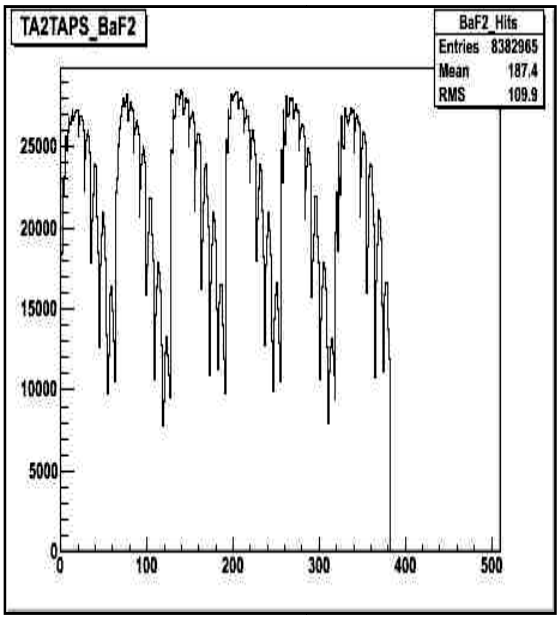

Figure 6.51: Our result of the position of elements of the 384elements of BaF_2crystal in virtual TAPS

Fig. 6.50 and Fig. 6.51 show that position of elements of 384 elements of NaI crystal in virtual TAPS detector. Both experimental result Fig. 6.50 and Monte Carlo simulation result Fig. 6.51 are in quite agreement. *TAPS* was designed with the purpose to study high-energy photon beams as well as neutral mesons.

6.4.3 Mass of eta meson comparison

We compared the graph of mass of *eta meson* obtained by McNicoll, Eilidh F [12] with our result obtained by using Monte Carlo Simulation. The graphs are shown below for the purpose of comparison.

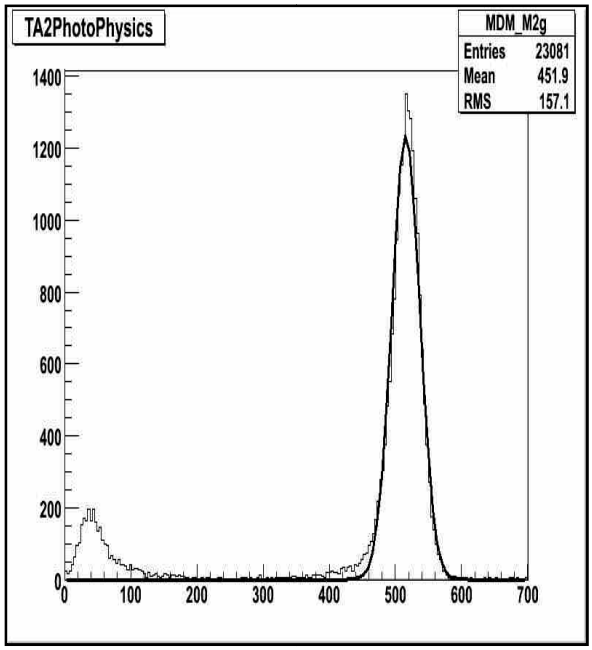

Figure 6.52: Our result of mass of eta

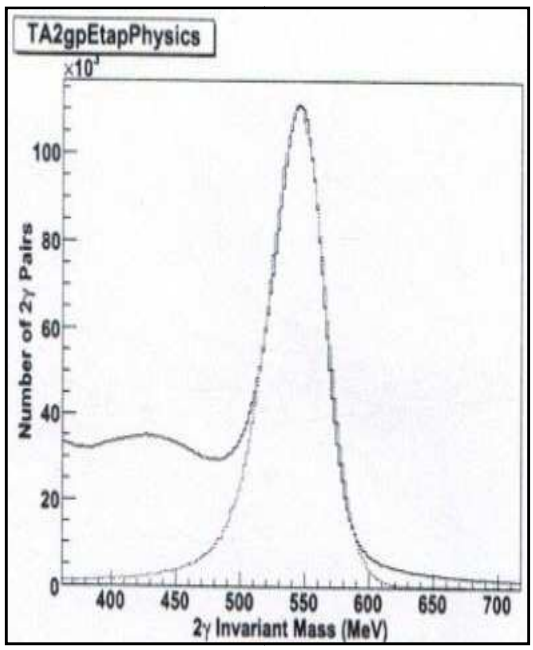

Figure 6.53: Mass of eta curve obtained by McNicoll in 2010 [12]

From these graphs, the nature of the curves found to be similar i.e. peak of the both mass of proton curves is approximately **550.095 MeV/c^2** and our result is in good agreement with the previous result. In Fig.6.52**,** indicates our result of mass of two gamma after applying *Gaussian distribution* and Fig.6.53 is mass of eta curve obtained by McNicoll in 2010.

6.4.3 Mass of proton comparison

Similarly we compared the graph of mass of proton obtained by McNicoll, Eilidh F [9] with our result. The graphs are shown below for the purpose of comparison.

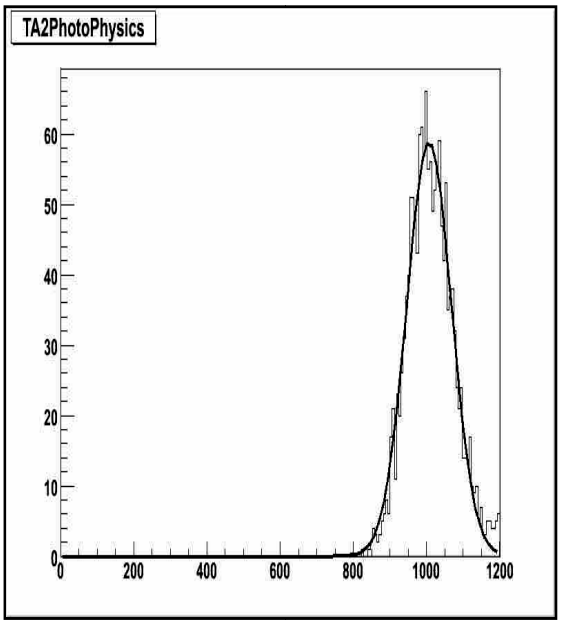

Figure 6.54: our result of mass of proton curve obtained by using Monte Carlo Simulation method

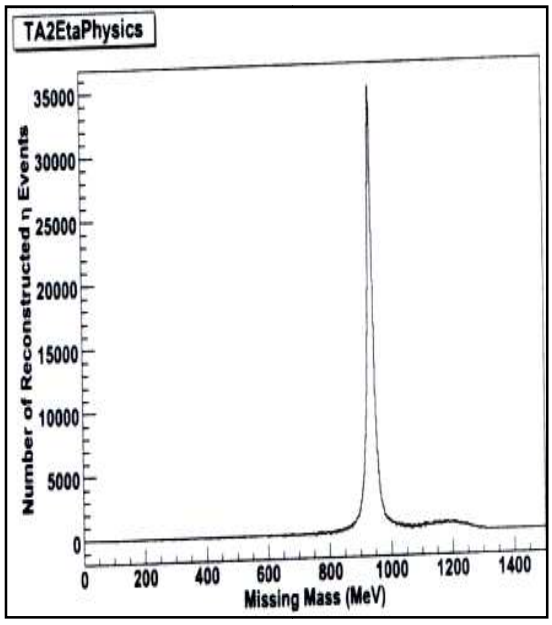

Figure 6.55: Mass of proton curve obtained by McNicoll in 2010 [7]

From these graphs, the nature of the curves found to be similar. Both curves has peak near to the mass of *proton* i.e. **938.27 MeV/c^2** and our result is in good agreement with the previous works.

6.5 Summary and conclusions

In this dissertation, we have studied the reaction of $\gamma p \rightarrow \eta p \rightarrow \gamma\gamma p$. This reaction accomplished by using **Monte Carlo Simulation** method. In our simulation method virtual experimental set up was designed. Choosing suitable value for the energy of the photon beam, we made different *dat* files. These files were run under *mkin* software and events were generated. Important generated events in the form of histograms were generation of *photon beam*, *eta meson*, *proton*, two *photons* and *target vertex*. These generated events were detected by using *cbsim* software. In this section, we observed histograms related with identification of particles, vertex, beam. Position of elements of virtual detectors i.e. *Crystal Ball* ad *TAPS* were also detected. After that, we reconstructed events by using *AcquRoot* software. From reconstruction, we studied histograms of *mass of eta meson, mass of proton, thetaCM* curves and position of elements of detectors.

From the reconstructed events invariant mass of *eta meson* and missing mass of *eta meson* or *proton mass* was found approximately **547 MeV/c^2** and **938 MeV/c^2**, respectively, which were expected results. *Mass of proton* curve and *eta meson* curve were studied by applying *Gaussian distribution*. Moreover, histograms of position of elements of NaI crystal in Crystal Ball and BaF_2 crystal in TAPS obtained from *cbsim* software and *AcquRoot* software closely matched. At final, we compared our results with the results obtained from previous simulation as well as experimental works and both results were found similar. Our study of *eta meson* production from **Monte Carlo Simulation** will be very helpful for the determination of important features e.g. *acceptance*, *tagging efficiency*, differential and total *cross section measurements* of $\gamma p \rightarrow \eta p$ reaction.

Bibliography

[1] J. Chadwick. **PRSL** A136, 692 (1932).

[2] Cornel, Hapegan. *On the isobaric spin and the scattering matrix,* Romanian Academy Institute of Atomic Physics, Bucharest, Romania proceedings of the, Series A Volume 3, Number 3/2002.

[3] Antonino, Zichichi. *From the Yukawa particle to the QWCG,* international nuclear physics conference, Tokyo, Japan, June 3-8, 2007.

[4] Tayal, D.C.. *Nuclear Physics,* New Offset Printers, New Delhi, (chapter 16,page 583-648), Reprint 2004.

[5] Murugeshan, R. *Modern Physics,* S Chand and Co. Ltd., Ram Nagar, New Delhi, Thirteenth Edition(chapter 38,page 534-545), 2007.

[6] Benson, Harris. *University Physics*, John Wiley & Sons, Inc., Singapore Ptd. Ltd. 2004.

[7] Wilson, Fred L.. *Fermi's theory of beta decay,*American journal of physics, **B** ol.36 , No. 12,December 1968.

[8] M. Gell-Mann, Phys. Lett. **8**, 214 (1964).

[9] Zweig, George. *Origins of the Quark Model* , Calt-68-805 Doe research and development report, 1980.

[10] Sears, Zemansky's, hugh D. Young, *University Physics,* Tata McGraw-Hill Company Ltd. Fourth Edition, 1974.

[11] www.slac.stanford.edu/BFROOT/www/Computing/Environment

/NewUser/htmlbug/node51.html last accessed 22/02/2012

[12] McNicoll, Eilidh F. *Eta photoproduction study with the upgraded Glasgow tagger at MAMI.* PhD thesis, University of Glasgow: Scotland, 2010.

[13] Bantawa, Kabi R. *Photoproduction of neutral kaons on deuterium.* PhD thesis, Kent State University, 2009.

[14] Jackson, John David. Classical Electrodynamics, Third edition, John Wiley & Sons., New York, 1998.

[15] Krik T. McDonald, *Neutral pion Decay*, Princeton University (1976).

[16] J. Berger *et al*., Physics. Rev. Lett. 61, 919 (1988).

[17] F. Plouin *et al*., Phys. Lett. **B276 ,** 526 (1992).

[18] R.S. Kessler *et al*., Phys.Rev. Lett. **70 ,** 892 (1993).

[19] C. Peng *et al*., Phys. Rev. Lett. **63**, 2353 (1989).

[20] Lee, Frank X.*Quasifree Eta Photoproduction from Nuclei*, TRI-PP-95-87/MKPH-T-96-2:

[21] S.A.Dytman *et al*.Bull.Am.Phys.Soc.**35** (1990) 1679 and contribution to the Fourth Conf. on the Intersection of Particle and Nuclear Physics.Tueson, 1991.

[22] S. Homma *et al*.J.Phys.Soc.Japan **57,** 828 (1998).

[23] Dugger, Michael. *Eta(547) and Eta(958)meson photoproduction on the proton*, PhD thesis, Arizona State University, 2001.

[24] Jason, William Brudvik. *Measurement of the branching ratio for eta-meson decay into a neutral pion and two photons*, PhD Thesis, University of California: Los angeles, 2007.

[25] A. Jankowiak *et al.*, EPAC 2006, Edinburgh, Scottland, p. 834 (2006).

[26] A. Jankowiak *et al.*, EPAC 2002, Paris, 1085 (2002).

[27] E.D. Bloom and C.W. Peck, Ann. Rev. Nucl. Part. Sci. **33**, 143(1983).

[28] R. Novoty, IEEE Trans. Nucl. Sci. **33**, 379 (1991).

[29] Annand, J. R. M.. Data Analysis within an AcquRoot Framework, University of Glasgow (2008).

[30] T. Feuster and U. Mosel, Phys. Rev. C **59**, 460 (1999).

[31] http://en.wikipedia.org/wiki/Monte_Carlo_method last accessed 18/03/2012.

[32] R. Brun and F. Rademakers et al., ROOT User's Guide 4.16 CERN, (2006).

[33] Gupta S.C. & Kapoor V. K., *Fundamentals of mathematical stastistics*, s. Chand & Sons.,New Delhi,August 2001.

Appendix A

A.1 dat file

The file name is *newetagama_1400.dat*.

0	! Startup Seed. gamma p -> pi0 p	*Row 1*
F 0 0 0 F	! Select (T/F)?, hid_cs, hid_ang, cm_var, err_check (T/F)?	*Row 2*
1	! Beam Particle GEANT id	*Row 3*
1.400 0.1	! Beam momentum, dP/P (std. dev., %)	*Row 4*
.2 .2	! Beam Sigma(x), Sigma(y) (std. dev., cm)	*Row 5*
0.5 0.5	! Beam Sigma_ThX, Sigma_ThY (std. dev., mrad)	*Row 6*
14 5.0	! Target Particle GEANT id, Target Length (cm)	*Row 7*
FALSE	! Use a distribution function?	*Row 8*
17 TRUE 0	! Part. id#histogram id# eta ① particle	*Row 9*
14 FALSE 0	! Part. id#, decay logical # proton ② particle	*Row10*
-1	! Terminate list of decay products	*Row11*
FALSE 0.0 180.0 0.0 360.0	! Limit CM angular range?	*Row12*
1 FALSE 0	!photon ③ particle, decay product of eta	*Row13*
1 FALSE 0	!photon ④ particle, decay product of eta	*Row14*
-1	! Terminate list of decay products	*Row15*
FALSE 0.0 180.0 0.0 360.0	! Limit CM angular range?	*Row16*

Explanation:.

Row 3: **1**! Beam particle GEANT id represents striking particle is gamma

Row 4: **1 .400** represents the energy of striking particle gamma is 400 MeV

Row 7: **14** represents GEANT id of target i.e. liquid hydrogen, 5 target length between striker and target

Row 9: **17 TRUE**: after striking *eta* is produced and TRUE means it further breaks

Row 10: **14 FALSE** means proton is produced and FALSE means it does not break

so in first case after striking liquid hydrogen by gamma eta and proton are produced.

$$\gamma p \rightarrow \eta p$$

Row 13: 1 FALSE means *eta* breaks into 1st photon and photon does not break further

Row 14 : 1 FALSE means eta breaks into 2nd photon and photon does not break further

so our final reaction becomes in the form of

$$\gamma p \rightarrow \eta p \rightarrow \gamma\gamma p$$

In above file **1.400** represents energy of incident gamma ray is **1400 MeV**. 1! Beam particle **GEANT id** represents gamma strikes liquid hydrogen target is symbolized as **GEANT id 14.** After striking by *gamma eta particle and proton* produced, this is represented as **17 TRUE** for eta and **14 FALSE** for proton. Symbol **TRUE** means eta particle is further breaks and FALSE means proton does not break. Eta breaks into two gammas in succession which is represented as **1 FALSE.**

Appendix B

B.1 mkin file

if ($# != 1) then

echo "ERROR: Must input either nothing (which runs all targets and \

energies), 'eg' which uses a specific Energy Channel and \

energy range."

echo " 'mkin_cb.sh 900'"

echo " or 'mkin_cb.sh ....MeV'"

exit 0

endif

set inc = 35

set eg = $1

#set eg = 1320

#set end = 1000

set end = 1400

if($eg> $end) then

echo "ERROR : eg >end"

exit 0

endif

if($end > 1500) then

echo "Error : end > 1400 MeV"

exit 0

endif

while($eg <= $end)

setmkin_file=/home/suman/mami_mcarlo/results_deckin/deckin_newetagama_$eg.hbook

if(! -e $mkin_file) then

echo "Input files $mkin_file doesnot exit . skkipping ....."

set eg = `expr $eg + $inc`

continue

endif

set cb_file = /home/suman/mami_mcarlo/results_cbsim/

new_krisg.$eg.hbook

set root_file = /home/suman/mami_mcarlo/results_cbsim/new_krisg.$eg.root

setenv FFCARDS /home/suman/mami_mcarlo/jb_ffcards_files/gamaeta.ffcards

setenv NTTITLE $cb_file

setenv INPUTFILE $mkin_file

setenv OUTPUTFILE $cb_file

cd /home/suman/mami_mcarlo/cbsim

./crystalball

h2root $cb_file $root_file

wait

set eg = `expr $eg + $inc`

end

end

exit 0

Inside mkin file bold letter places and italic letter places represent our correction.

Appendix C

C.1 gammaeta. ffcards

LIST

c FFREAD system card that causes the data cards and their values to be

AUTO 0

c GEANT data card that controls whether tracking medium parameters are

FREQ 5000

c frequency of updates on the simulation's progress. 0 (default) or a

SEED 0

SMEA TRUE

c switches on (TRUE, default) or off (FALSE) the 2% x E^(-1/4) energy

SPLT 0.0 0.0 0.0

TMAT 3

c target material. The default value is 3 for liquid hydrogen. Other

TRAC FALSE FALSE TRUE 97*TRUE

cTRAC FALSE 98*TRUE

c an array of 99 logical variables specifying whether particles are

TRGT TRUE

GAP 0.05 0.05

HPAC 0

GEOB 0 0 0 0

CUTS 0.0001 0.0001 0.001 0.001 0.001 0.0001 0.0001 1E4 1E4 0.01 0.5E-6

STOP

TMAT 3 represents default value of target liquid hydrogen. In **TRAC FALSE FALSE TRUE** means two gammas and one proton is produced in the final. In $\gamma p \rightarrow \eta p \rightarrow \gamma\gamma p$, **FALSE FALSE** means η breaks into two gamma and TRUE means proton remains same in the final.

Appendix D

D.1 CBMC.offline

Name: h12 22 MC

Branch: npart 4

Branch: dircos 2048

Branch: plab 1024

Branch: elab 1024

Branch: idpart 1024

Branch: vertex 12

Branch: beam 16

Branch: nhits 4

Branch: ecryst 1024

Branch: icryst 1024

Branch: enai 4

Branch: vhits 4

Branch: eveto 1024

Branch: iveto 1024

Branch: etot 4

Branch: eleak 4

Branch: ntaps 4

Branch: ictaps 1024

Branch: ectapsl 1024

Branch: ectapfs 1024

Branch: tctaps 1024

Branch: evtaps 1024

TreeFile: /home/suman/mami_mcarlo/results_cbsim/new_krisnewg.1400.root

SetADC: 29001 0   12

Analysis: TA2UserAnalysis

AnalysisSetup: CBMCanalysis.dat

Appendix E

E.1 Gaussian distribution

One of the most important probability distribution, which has wider applications, is the Gaussian distribution. This distribution is also called Normal distribution. In this distribution the variate x has following distribution of the form

$$p(x) = \frac{1}{\sigma\sqrt{2\pi}} e^{-\frac{1}{2}\frac{(x-\mu)^2}{\sigma^2}}\, dx, \quad -\infty \leq x \leq \infty$$

$p(x) = f(x)dx$ when

$$f(x) = \frac{1}{\sigma\sqrt{2\pi}} e^{-\frac{1}{2}\frac{(x-\mu)^2}{\sigma^2}} \qquad (a)$$

y= f(x) is called normal probability curve.

when $z = \frac{x-\mu}{\sigma}$, $P(z) = \frac{1}{\sqrt{2\pi}} e^{-\frac{1}{2}} z^2\, dz$ (b)

z is called standardize normal variate.

Chief features of Gaussian or Normal distribution

(1) The curve is bell shaped and symmetrical about limit x=μ.

(2) Mean, Median and mode of the distribution coincide.

(3) As x increase numerically , f(x) decreases rapidly. The maximum probability at point x=μ and given by

$[P(x)]_{max} = \frac{1}{\sigma\sqrt{2\pi}}$ [33]